5

MARTIN MARIETTA ENERGY SYSTEMS LIBRARIES
3 4456 0361286 5

CENTRAL RESEARCH LIBRARY
DOCUMENT COLLECTION

ORNL-2582
Metallurgy and Ceramics

cy. 5

THE EFFECT OF SIMULATED WELD THERMAL CYCLES ON THE PROPERTIES OF HASTELLOY B

E. G. Thompson

CENTRAL RESEARCH LIBRARY
DOCUMENT COLLECTION
LIBRARY LOAN COPY
DO NOT TRANSFER TO ANOTHER PERSON
If you wish someone else to see this document, send in name with document and the library will arrange a loan.

OAK RIDGE NATIONAL LABORATORY
operated by
UNION CARBIDE CORPORATION
for the
U.S. ATOMIC ENERGY COMMISSION

LEGAL NOTICE

This report was prepared as an account of Government sponsored work. Neither the United States, nor the Commission, nor any person acting on behalf of the Commission:

A. Makes any warranty or representation, express or implied, with respect to the accuracy, completeness, or usefulness of the information contained in this report, or that the use of any information, apparatus, method, or process disclosed in this report may not infringe privately owned rights; or

B. Assumes any liabilities with respect to the use of, or for damages resulting from the use of any information, apparatus, method, or process disclosed in this report.

As used in the above, "person acting on behalf of the Commission" includes any employee or contractor of the Commission to the extent that such employee or contractor prepares, handles or distributes, or provides access to, any information pursuant to his employment or contract with the Commission.

ORNL-2582
Metallurgy and Ceramics

Contract No. W-7405-eng-26

METALLURGY DIVISION

THE EFFECT OF SIMULATED WELD THERMAL CYCLES ON THE PROPERTIES OF HASTELLOY B

Ernest G. Thompson

DATE ISSUED

OCT 14 1958

OAK RIDGE NATIONAL LABORATORY
Oak Ridge, Tennessee
operated by
UNION CARBIDE CORPORATION
for the
U.S. ATOMIC ENERGY COMMISSION

MARTIN MARIETTA ENERGY SYSTEMS LIBRARIES
3 4456 0361286 5

ACKNOWLEDGMENTS

A Thesis submitted to the Faculty of the Department of Metallurgical Engineering, Rensselaer Polytechnic Institute, Troy, New York, June 1956, in partial fullfillment of the requirements for the degree of Master of Metallurgical Engineering.

This work was performed under Union Carbide Corporation Subcontract No. 371, and was administered under the direction of the Metallurgy Division, Oak Ridge National Laboratory.

The author is indebted to Dr. Ernest F. Nippes and Dr. Warren F. Savage for their invaluable counsel, and to Messrs. Edward Pigan and Robert Allio for assistance in the actual testing program.

TABLE OF CONTENTS

		Page
ABSTRACT		1
I.	INTRODUCTION	2
II.	HISTORICAL REVIEW	5
	Background	5
	Studies of Nickel-Molybdenum Alloys	6
	Weldability of Hastelloy B	8
III.	THE HOT DUCTILITY DEVICE	9
	Introduction	9
	Performance Specifications	9
	The Time-Temperature Controller	10
	The Loading Device	12
	Recording Instrumentation	16
	Measuring Instrumentation	16
IV.	MATERIAL	19
V.	EXPERIMENTAL PROCEDURE	20
	Manufacture of Specimens	20
	Identification of Specimens	20
	Testing of Specimens	20
	Collection of Data	22
VI.	RESULTS	27
	Introduction	27
	Reduction-In-Area Data	27
	Tensile Strength Data	40
	Strain Data	40
	Metallographic Observations	41
VII.	DISCUSSION	58
VIII.	CONCLUSIONS	62
LITERATURE CITED		64

ABSTRACT

This thesis has, as its purpose, the investigation of the effects of weld thermal cycles in the temperature range of 1500°F to 2400°F on the properties and microstructure of the weld heat-affected zone of Hastelloy B. Through the use of a time-temperature controller and a hydraulic-mechanical testing device, specimens of a size suitable for study were subjected to simulated weld thermal cycles and fractured at various points during these cycles. Reduction-in-area, load, and strain measurements were taken and the results correlated with microstructural changes occurring as a result of the thermal cycles involved.

The as-received structure of the material was found to be a nickel-rich solid solution of molybdenum (α) and a single secondary phase concluded to be an intermetallic compound NiMo (δ).

Hastelloy B suffered no impairment of its ductility properties as a result of thermal cycles up to 2250°F in maximum temperature. At 2300°F the material began to lose its ductility and at 2350°F and 2400°F it was, to all intents, completely brittle.

Specimens of Hastelloy B were tested during the cooling portion of 2300°F, 2350°F, and 2400°F thermal cycles. The peak temperature of 2300°F was found to cause no impairment in the ductility of Hastelloy B at lower temperatures, the 2350°F peak temperature caused permanent injury to the material in the range of 2300°F, and the 2400°F peak temperature was found to injure the material slightly from 1800°F to 2000°F and to embrittle it severely at higher temperatures.

No unusual effects were noted from tensile strength measurements and only the 2400°F thermal cycle affected this property, causing about a 10% loss in tensile strength at all testing temperatures.

Strain measurements were found to be insensitive as a measure of the effect of weld thermal cycles on the material.

The loss in ductility at high temperatures for a thermal cycle involving a maximum temperature of 2350°F was attributed to the formation of grain-boundary films. The severe loss in ductility and mild loss of tensile strength as a result of the 2400°F thermal cycle was concluded to be caused by the formation of a eutectic along the grain boundaries of the material.

From the tests conducted, it was further concluded that the eutectic formed at a minimum temperature of 2350°F and from its effect on the ductility of Hastelloy B, that the eutectic must be weaker than the higher melting matrix at temperatures above 2000°F.

PART I

INTRODUCTION

As a result of World War II, which saw the birth of the jet airplane and the atomic bomb, a greatly increased demand has been created for alloys resistant to high temperatures and corrosion. The initial impetus in the use of "super alloys" furnished by the military has increased steadily in the years since the war, due to both governmental and commercial demands.

Such demand has brought intensive engineerning and scientific talent to bear on the development of materials capable of withstanding operating conditions at the higher temperatures encountered by supersonic aircraft or in atomic reactors.

As a natural occurrence, the initial problem has produced a host of associated problems, among them the forming and fabrication of the materials involved. Particularly, nuclear technology, which demands essentially 100% leak-proof equipment, has concentrated considerable effort on welding techniques as the only suitable means of fabrication.

Because the weldments of stainless steels and nickel-base and cobalt-base alloys are more prone to cracking than those of many other materials, much effort has been expended in attempts to determine the causes of these weld cracks. Since the fractures are intergranular in nature, cracking has been attributed to brittle or low-melting grain-boundary films. Unfortunately, investigations to date have proved little and are sometimes conflicting in results. It was therefore decided to investigate the effects of rapid weld thermal cycles on the properties and microstructure of the heat-affected zones of stainless steels and high-temperature alloys in an attempt to determine the basic mechanism (or mechanisms) behind cracking in this area associated with welding.

This thesis presents only what has been learned in this investigation about Hastelloy B. Simulated weld specimens have been produced by subjecting suitably designed samples to rapid weld thermal cycles involving peak temperatures of 1500 to 2400°F and fracturing the samples during these cycles.

All test specimens were produced by the Rensselaer Polytechnic Institute time-temperature controller.[1] Data accumulated include reduction-in-area measurements, ultimate tensile strength, and total strain of each sample. A metallographic study of representative specimens is presented in an attempt to correlate microstructural changes with changes in other properties.

PART II

HISTORICAL REVIEW

Background

Some years ago it was decided by the staff of the welding laboratory at Rensselaer Polytechnic Institute that more science should be introduced into the art of welding. With this thought in mind, research was conducted[2,3] to measure the actual thermal cycles experienced by different points in the heat-affected zone adjacent to a weld as the bead was being layed. Results of these measurements were correlated with a mathematical formula[4] previously published, and modifications were made in the formula to fit the experimental data. From these investigations, families of curves were drawn of the actual thermal cycles experienced in planes parallel to, and at varying distances from the fusion zone.

The next step in this long-range program to study welding from a more basic approach than previously attempted was to construct a time-temperature controller[1] capable of duplicating the established weld thermal cycles in specimens of a suitable size for studies of the structures and properties resulting from various thermal conditions. This was accomplished and the initial investigation[5] using the time-temperature controller and a converted flash welder to produce Charpy V-notch specimens was a study of the impact properties of different areas of the heat-affected zone for 5/8-in. ASTM specification A-201 aluminum-killed steel. This study was followed by another[6] which investigated changes in microstructural, tensile, and impact properties throughout the heat-affected zone of AISI 347 stainless steel. The last step thus far taken in this long program has been the development of a device[7] permitting a study of the effects of temperature and prior thermal history on the hot ductility of structural alloys.

The preceding history should furnish a picture of what is presently being attempted in welding research at Rensselaer Polytechnic Institute. This report is a continuation of the "Hot Ductility" studies[7] published this past year.

Studies of Nickel-Molybdenum Alloys

Hastelloy B has been produced commercially since about 1927, primarily for its corrosion resistance to various media, though it was known that the alloy also had good high-temperature properties. Except for its corrosion-resistant properties, comparatively little was known about this alloy until recent years.

Ellinger's[8] research on the Ni-Mo system has given a sound foundation on which to build up knowledge of Hastelloy B. In a comprehensive study of the system, he reported a phase diagram very similar to Figure 1.[9] He also investigated in this report the age-hardening characteristics of Ni-Mo alloys containing from 21 to 35% molybdenum at 2% intervals, reporting these compositions as falling into two groups: (1) those which harden by precipitation of β phase (Ni_4Mo) in α solid solution and (2) those hardening by decomposition of the supersaturated α phase to γ (Ni_3Mo) and β.

A recent report by Monkman, Grant, and Floe[10] investigated the effect of vacuum melting and compositional variations on the ductility, mechanical, and stress-rupture properties of nickel-molybdenum alloys ranging from 17.3 to 36.0% Mo. A sample of commercial Hastelloy B was included in the investigation for comparison purposes. Test results showed that Hastelloy B was among the best in these properties and was also the most stable, being unaffected by long-time exposures at 1350, 1500, and 1650°F. While this stability factor was not investigated, it was attributed to minor amounts of alloying elements present.

In an investigation to determine minor phases present in high-temperature alloys,[11] Rosenbaum reports only a carbide of the composition M_6C (where M stands for any element) identifiable in Hastelloy B.

A symposium[12] by the ASTM described the use of Hastelloy B for gas turbine applications during the war. Reasons for its use were availability, high-temperature strength, and resistance to oxidation up to 1400°F.

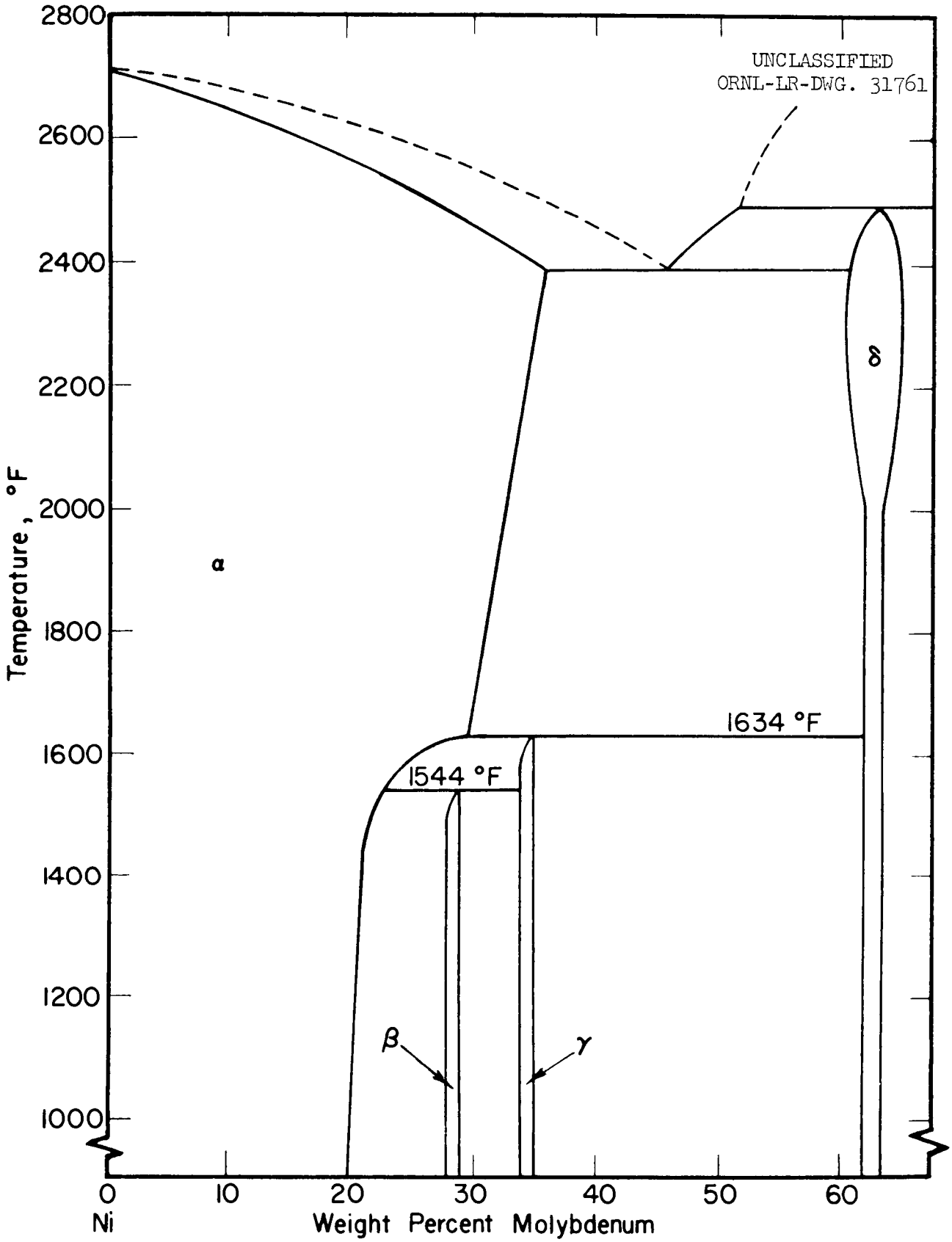

MOLYBDENUM-NICKEL PHASE DIAGRAM BY R. M. PARKE

FIGURE 1

Weldability of Hastelloy B

The only report[13] found relating directly to the weldabilty of Hastelloy B was published recently by the Mond Nickel Company. An investigation was conducted to determine the reason for the susceptibility of the weld heat-affected zone of Corronel B (the British version of Hastelloy B) to intergranular corrosion. This susceptibility was found to be associated with a dispersed phase which was extracted and identified as a carbide of the M_6C type. By powder metallurgical means, single-phase alloys were produced containing less than 0.01% each of carbon and silicon. These alloys were immune to intergranular attack after welding.

No literature concerned with particular welding fabrication problems or investigations of service failures could be found. The writer was verbally informed, however, by representatives of the sponsor that Hastelloy B was difficult to weld and many problems had to be surmounted.

PART III

THE HOT-DUCTILITY DEVICE

Introduction

The time-temperature controller,[1] a device previously developed by the welding laboratory of Rensselaer Polytechnic Institute for the study of the effects of rapid thermal cycles on the properties of various materials,[6,7,8] was modified by the addition of a hydraulic loading device to test the hot ductility of samples subjected to a variety of weld thermal cycles. Recent refinements to this equipment include the addition of a recording oscillograph, an SR-4 load cell, and a linear strain transducer.

Performance Specifications

The actual performance specifications[14] of the Hot-Ductility Testing Device in its present form are summarized below:

1. Heating rates up to 2000°F/sec. can be reproduced with an instantaneous accuracy of 15°F.
2. Cooling rates up to 300°F/sec. at 1300°F can be reproduced with an instantaneous accuracy of 15°F.
3. Thermal cycles having peak temperatures 50°F or more below the melting temperature of the material under test can be duplicated in metallic specimens of suitable size for testing, subject to the limitations in the heating and cooling rates set forth above.
4. The desired thermal cycle can be consistently duplicated to within 15°F in a volume of metal 1/4 in. in diameter and at least 1/4 in. long.
5. The specimen undergoing exposure to the desired thermal cycle can be fractured at any point in the thermal cycle by application of an axial tensile load.

6. The rate of application of the axial tensile load can be varied within limits, if desired.
7. Simply constructed sheet-metal cams serve to program the entire operation, permitting any reasonable thermal cycle of not over five minutes duration to be performed automatically.
8. The device in its present form utilizes specimens of the following dimensions:

   Length - 4 1/2 ± 1/8 in.

   Diameter - 0.250 + 0.000 in.
   - 0.001 in.

   (Threaded for 1/2 in. on each end with a 1/4-20 thread.)
9. Suitable means are provided for monitoring the entire operation to ascertain that the equipment is functioning properly.

The Time-Temperature Controller

Figure 2 is a schematic describing the hot-ductility device. This diagram shows a test specimen mounted in jaws so as to complete the secondary of a 38 Kva welding transformer. The jaws are made of Mallory No. 3 high-conductivity alloy and are designed similar to the well-known "Templin" grips used in tensile testing. Heat for the thermal cycle is provided by the resistance of the specimen to the flow of electrical current. Control of the cooling cycle is obtained by the water-cooled jaws.

An open-circuit, chromel-alumel thermocouple made of 10-mil wire is attached to the specimen by a percussion welding technique. The thermocouple serves both to control the specimen's thermal cycle and to record its temperature at rupture.

E_1, the output of the thermocouple, represents the instantaneous temperature of the specimen. This potential is bucked against E_2, representing the instantaneous temperature desired by the cam. E_3, the error signal, is the difference between E_1 and E_2. Being of a magnitude of 0.1 mv or less, it is fed into a high-gain amplifier which multiplies it approximately 500,000 times. A D.C. bias supply retains the thyratron grids negative so that fluctuations in line voltage do not misfire the thyratrons. This

UNCLASSIFIED
ORNL-LR-DWG. 31762

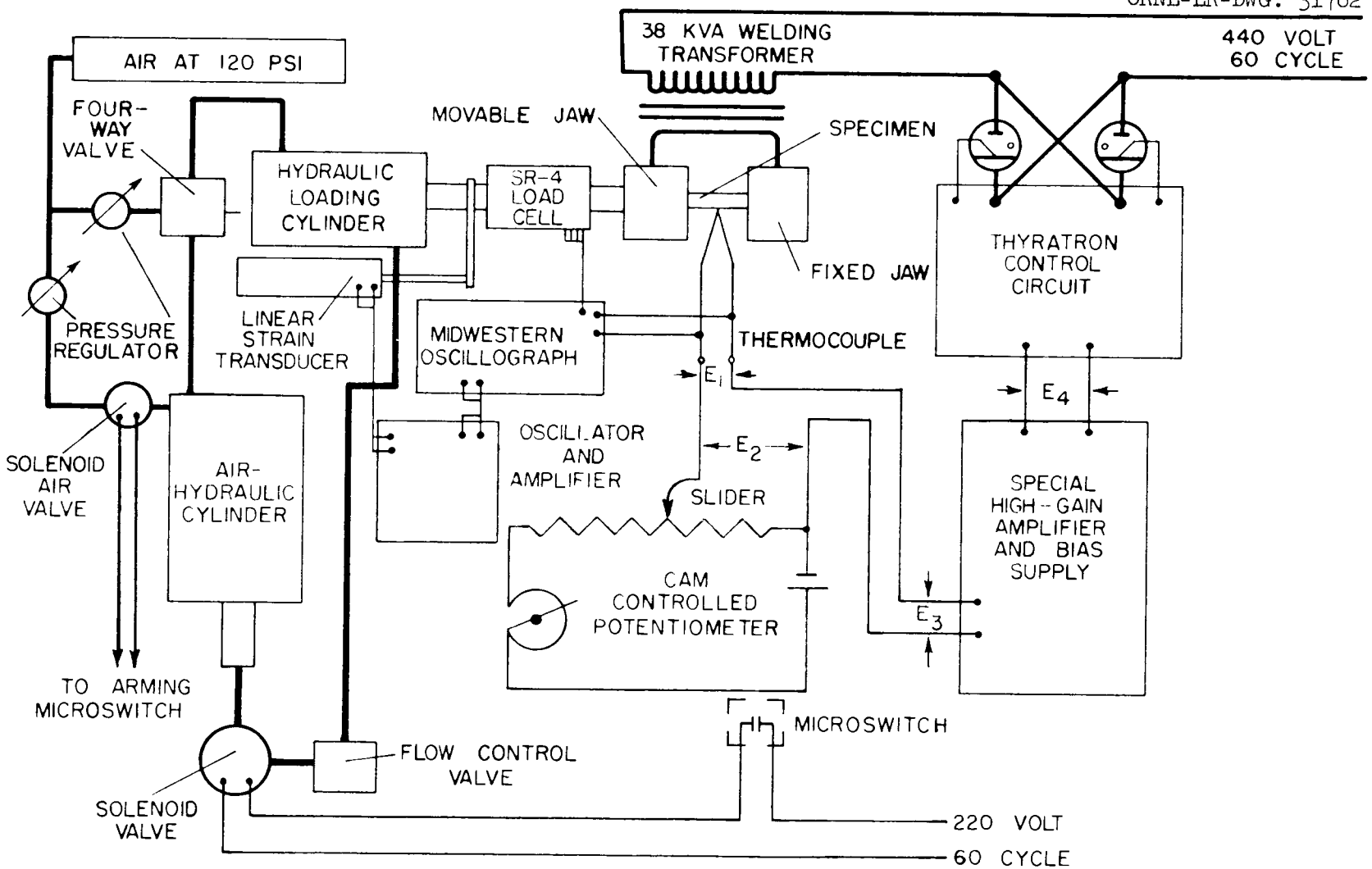

SCHEMATIC DIAGRAM OF HOT DUCTILITY EQUIPMENT

FIG. 2

negative bias must be overcome by E_3 before the thyratron control circuit fires. When the thyratrons receive a positive signal indicating that the test specimen is below temperature, they fire, and in turn cause the ignitron to fire a few microseconds later. The ignitrons energize the welding transformer primary and thereby send secondary current through the test specimen.

The cam-controller which programs the equipment may be seen in Figure 3. A sheet metal cam is positioned for a test run. The cam follower is visible near the end of the cam cycle. It consists of a pin mounted in a block which travels on ways. To the right of the cam follower is a multiple microswitch which is triggered by the cam follower. Its function will be explained later. In the foreground is a Brush recording oscillograph used to make a permanent record of the amplitude and frequency of the electrical pulses through the test specimen during a run.

Figure 4 is a view of the control panel of the time-temperature controller. The oscilloscope on the left is for the purpose of observing the instantaneous electrical input through the test specimen while a thermal cycle is in progress.

The Loading Device

The loading device consists of the equipment shown on the left side of Figure 2. The movable jaw is connected through an SR-4 load cell to the ram of a 2 1/2-in. diameter hydraulic cylinder. The fitting between the load cell and the movable jaw is of a self-aligning design so that only a uniaxial load is applied to the specimen.

The hydraulic cylinder is actuated by oil under 3000 psi pressure. Rate of oil flow is controlled by a constant flow control valve set to give the desired strain rate. The remaining equipment serves to build up air pressure of 120 psi to the required 3000 psi oil pressure. The loading cycle is initiated by a preset microswitch which is, in turn, triggered by the cam follower.

Figure 5 is a picture of the hot-ductility testing apparatus. The instrumentation mounted on the carriage at the left of the photograph is the recording equipment.

UNCLASSIFIED
PHOTO 44561

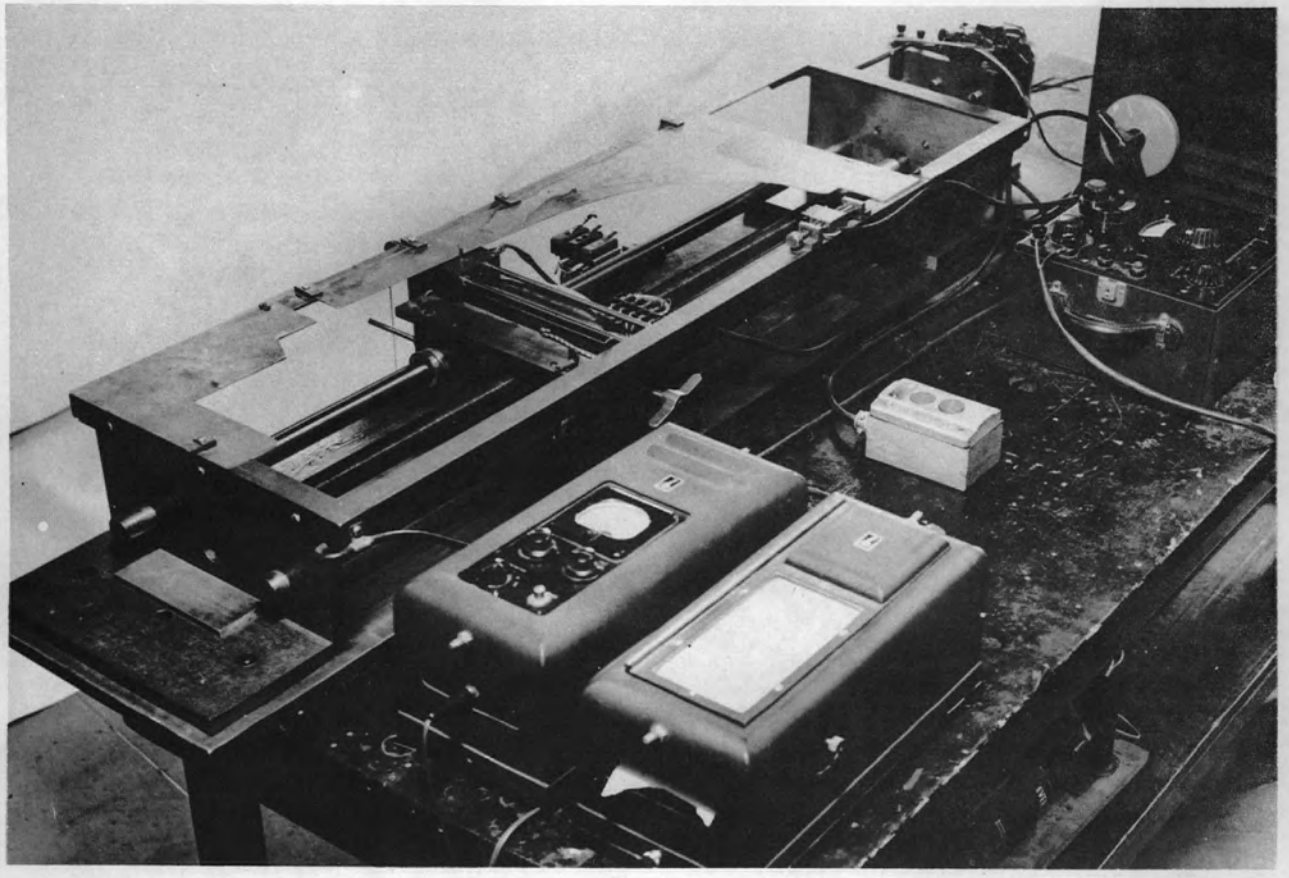

Fig. 3

Cam-Controller Monitoring the Test Cycle

UNCLASSIFIED
PHOTO 44562

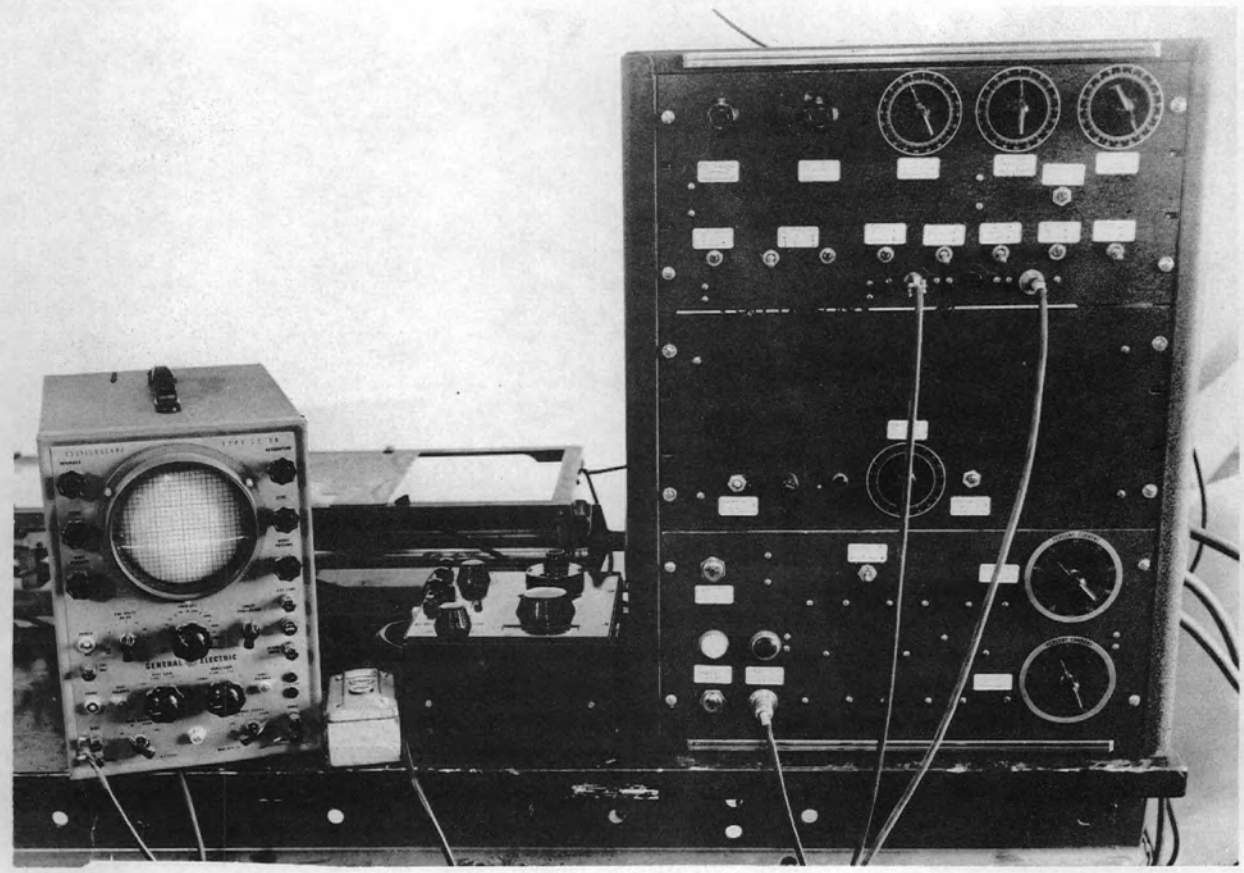

Fig. 4

The Control Panel of the Time-Temperature Controller

UNCLASSIFIED
PHOTO 44563

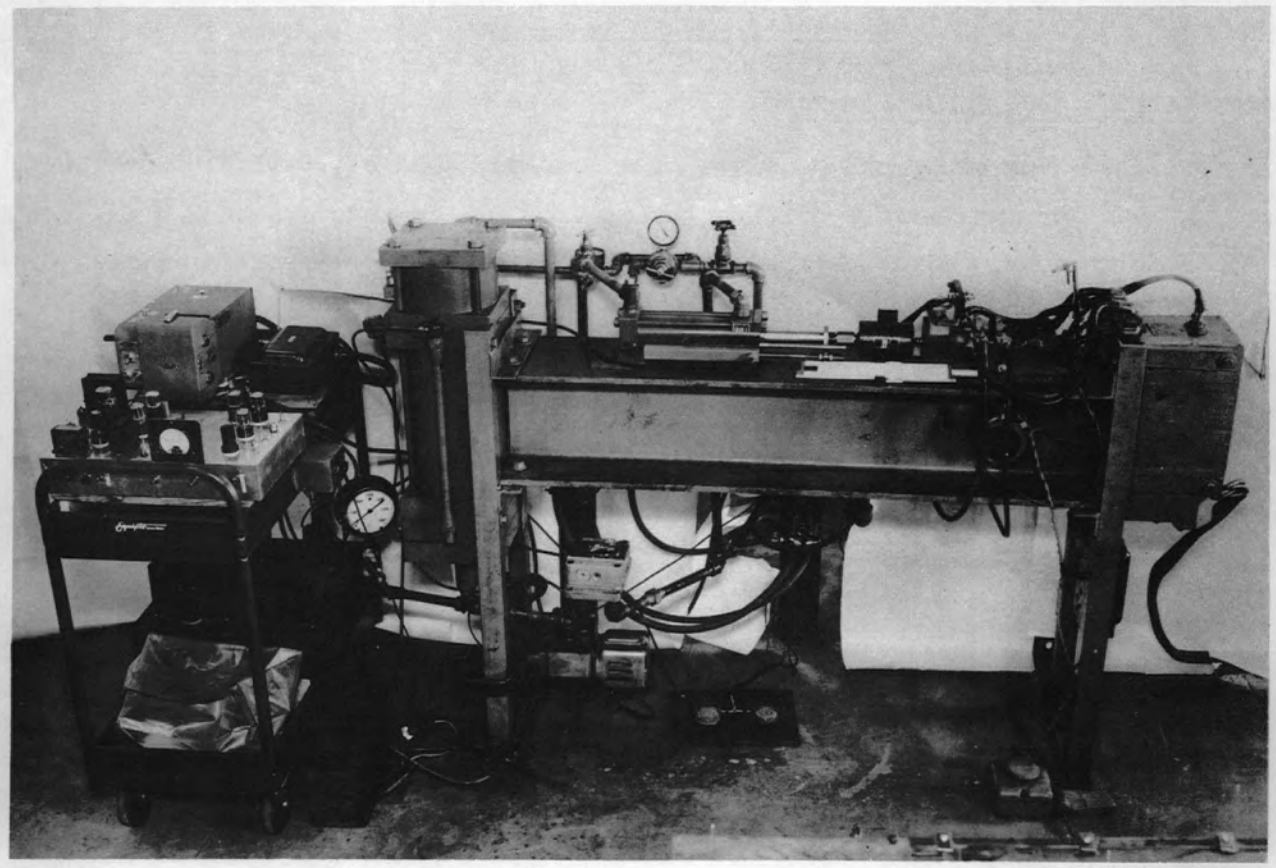

Fig. 5

The Hot Ductility Testing Apparatus

At the extreme right of the photograph is the primary of the welding transformer. To the left of it is the mounting station, consisting of the fixed and movable jaws. Immediately above the slide rule is an SR-4 load cell installed between the movable jaw and the hydraulic cylinder. Mounted in front of the hydraulic cylinder is a linear strain transducer. The vertical cylinder mounted on the left end of the hot-ductility tester is the air hydraulic cylinder which supplies the hydraulic loading cylinder.

Recording Instrumentation

Midwestern Model 580 Oscillograph

The recording equipment consists of a fourteen-channel, variable-speed oscillograph designed with recording speeds from 1/2 in./sec. to 44 3/4 in./sec. Simultaneously with test records, timing lines of 0.01 sec. intervals are recorded on the film.

At present, only four channels of the oscillograph are in use. One galvanometer records stress data, a second records strain data, the third records the temperature of the specimen at rupture, and the fourth is used as a reference line for calibration purposes.

A picture of the Midwestern Oscillograph is shown in Figure 6. It is the unit at the left rear of the carriage. The camera is mounted on front of the oscillograph ready for operation.

The amplifier in the foreground is part of the instrumentation of the strain transducer.

Measuring Instrumentation

Baldwin SR-4 Load Cell, Type U-1

The SR-4 resistance wire strain gages are connected in the form of a balanced Wheatstone bridge and bonded to a high-strength-metal column, the entire assembly being hermetically sealed. A constant voltage of approximately 6 volts is applied across opposite corners of the bridge so that a load applied to the cell changes the resistance of the gages, producing a

UNCLASSIFIED
PHOTO 44564

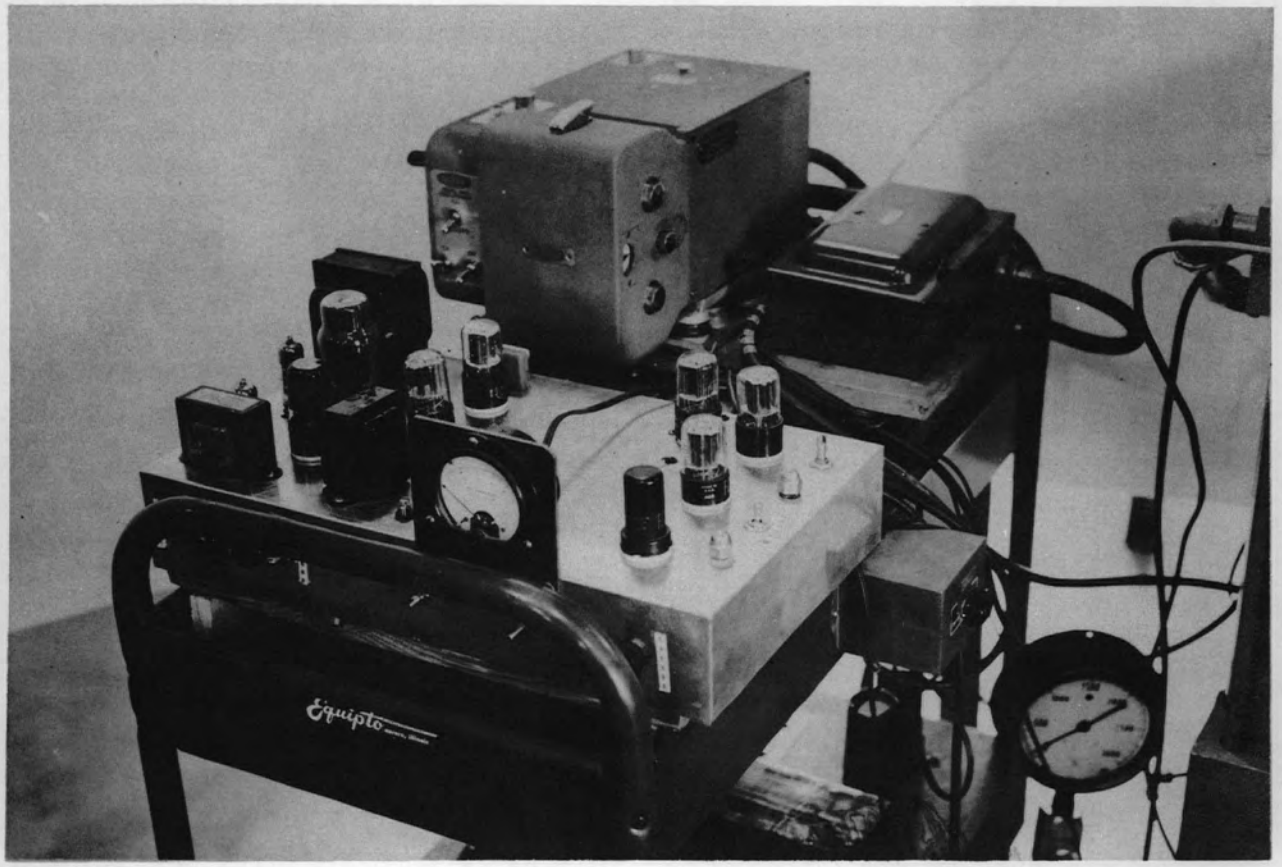

Fig. 6
The Recording Oscillograph

change in the output voltage from the bridge. This variation in output voltage under different loads is converted to galvanometer deflection by the recording oscillograph.

Cresent Model HC-2-4.0 Extensometer Micrometer

The measurement of strain occurring during the loading of a specimen to rupture is accomplished by a variable permeance transducer manufactured by the Crescent Engineering and Research Company.

The body of the instrument consists of two symmetrical precision coils connected in a bridge circuit. The coils are encased in plastic and hermetically sealed in a case. A probe is guided along an internal bore through the coils, the position of the probe determining the voltage output signal. An extension of the probe is connected by mechanical linkage to the hydraulic ram as shown in Figure 2.

With a test specimen in position, the probe is positioned equally in each coil, giving a zero output voltage signal. As the specimen is loaded, the probe is displaced by a distance equal to the travel of the movable jaw. The probe displacement unbalances the bridge, producing a continuous change in output voltage with changing position.

The output voltage of the strain transducer is amplified, rectified, and filtered before being sent to the recording oscillograph.

PART IV

MATERIAL

The Hastelloy B reported on in this thesis was supplied as 0.251-in. diameter cold-finished rod in 10-ft lengths. The chemical composition of this material is as given in Table I and the as-received mechanical properties are given in Table II.

TABLE I

CHEMICAL COMPOSITION OF HASTELLOY B

Heat No	Composition (wt %)										
	Cr	Fe	C	Si	Co	Ni	Mn	V	Mo	P	S
B1337	0.50	4.97	0.02	0.36	0.50	Bal.	0.42	0.37	27.04	0.007	0.008

TABLE II

AS-RECEIVED MECHANICAL PROPERTIES OF HASTELLOY B

Hardness	Yield Strength at 0.2% offset (psi)	Ultimate Tensile Strength (psi)
$96R_b$	66,000	135,000

PART V

EXPERIMENTAL PROCEDURE

Manufacture of Specimens

The raw material received was centerless ground to size and machined into finished specimens meeting the specifications previously stated.

Identification of Specimens

All specimens were identified with a letter-and-number code which was vibra-tool marked near both ends of every sample.

Testing of Specimens

Before start test runs, all samples were cleaned with acetone to ensure uniform contact resistance and good adherence of the thermocouples.

To maintain a constant test length, a specimen was set on a gage block and retention nuts were threaded on each end. The specimen was then removed from the gage block, set in the grips and inserted in the jaws of the hot-ductility apparatus. The use of retention nuts was also desirable to prevent possible slippage of the specimen in the grips when the load cycle was initiated.

Proper seating of the specimen in the jaws was ensured by applying a preload of 80 lb of compressed air to the movable jaw and then hammering the grips with a hard rubber mallet. After the specimen was satisfactorily seated, the preload was removed.

Next an open-circuit thermocouple was attached to the sample by individually percussion welding the chromel and alumel wires to the surface of the sample. The wires were spaced about 1/32 in. apart on the circumference. Their longitudinal position was automatically determined by the simple welding device shown in Figure 7. The thermocouple wire ends were then connected to the terminal block visible at the upper left corner of Figure 7. This completed the circuit to both the recording oscillograph and the cam-controller.

A cam duplicating the desired thermal cycle was set up to control the specimen. Then a triple microswitch was adjusted so that the cam follower would trigger it at the desired breaking temperature. This multiple microswitch functioned (1) to energize the solenoid air valve (see Figure 2) a few seconds

UNCLASSIFIED
PHOTO 44565

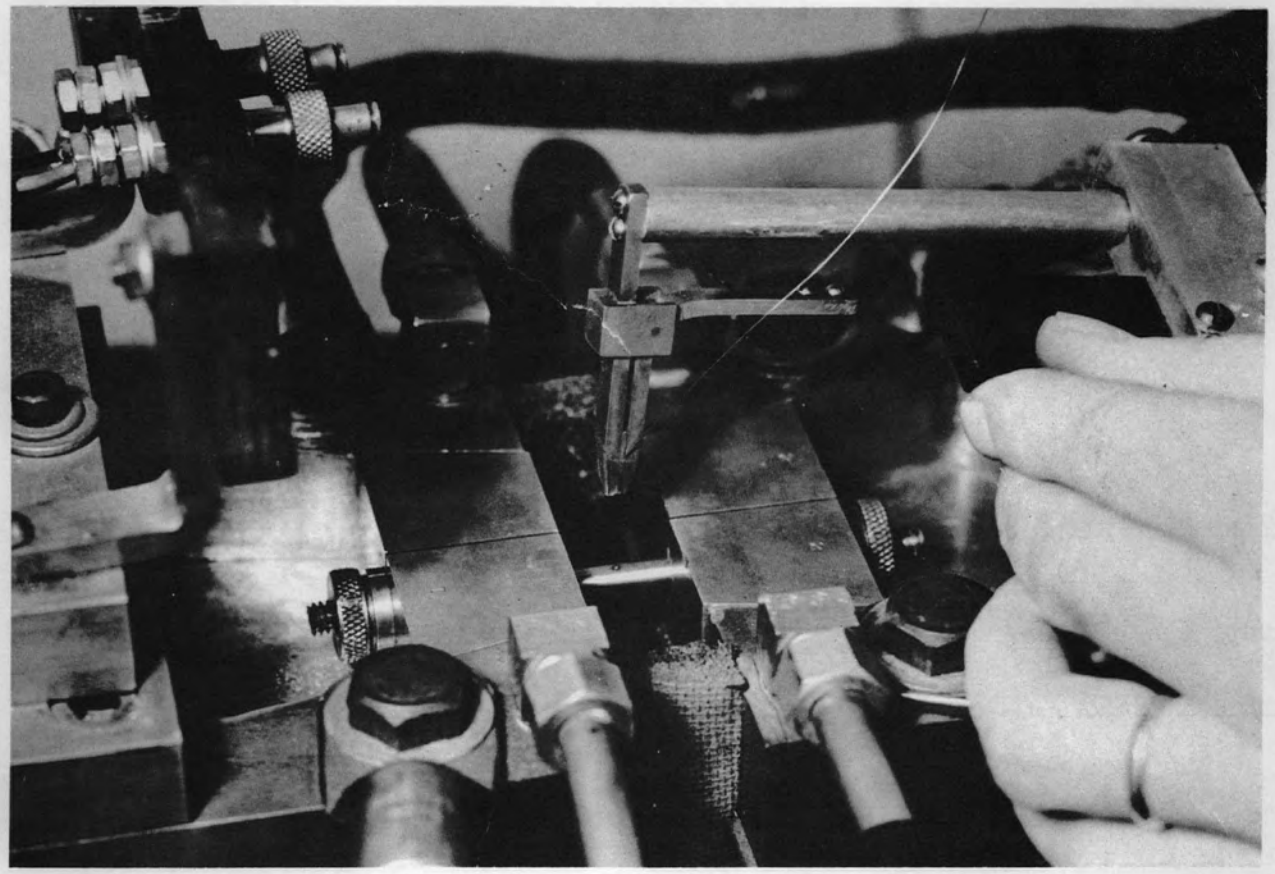

Fig. 7

Close-Up of Test Station Showing Welding
of Thermocouple Wire to Specimen

before loading the specimen, followed by (2) starting the oscillographic recording camera, followed by (3) initiating the hydraulic loading cylinder to rupture the specimen.

Next a low-temperature (400°F to 800°F) run was made to check the thermocouple for satisfactory performance. Regularly spaced, constant amplitude pulses of current as shown on a Brush recorder were indicative of satisfactory performance.

Assuming satisfactory thermocouple response, the cam cycle was initiated, all subsequent operations following automatically until the test sample was ruptured. A sample at elevated temperature during an actual test cycle is shown in Figure 8.

Specimens were tested during the heating portion of the thermal cycle at peak temperatures of 1500, 1800, 2000, 2200, 2250, 2300, 2350, and 2400°F. Specimens were cycled to peak temperatures of 2300, 2350, and 2400°F, then ruptured during the cooling portion of the thermal cycle at temperatures of 1500, 1800, 2000, 2200, and 2300°F. These weld thermal cycles and their location in the heat-affected zone of a weld are shown in Figure 9.[14]

Collection of Data

Calibration of Recording Galvanometers

All galvanometers were periodically calibrated. The methods of calibration are explained in the following paragraphs.

Load Galvanometer

The SR-4 load cell was mounted in a tensile machine and tensile load was applied to it in convenient increments, the galvanometer deflection for each valve of load being recorded. Thus, a curve of load versus galvanometer deflection could be drawn.

Since this method was inconvenient for rapid recalibration, a resistor box was made which was attached across one arm of the Wheatstone bridge of strain gages in the load cell. For each switch position of the resistor box, the bridge was unbalanced, producing an artificial load signal which was recorded as galvanometer deflection. In this manner, each switch

UNCLASSIFIED
PHOTO 44566

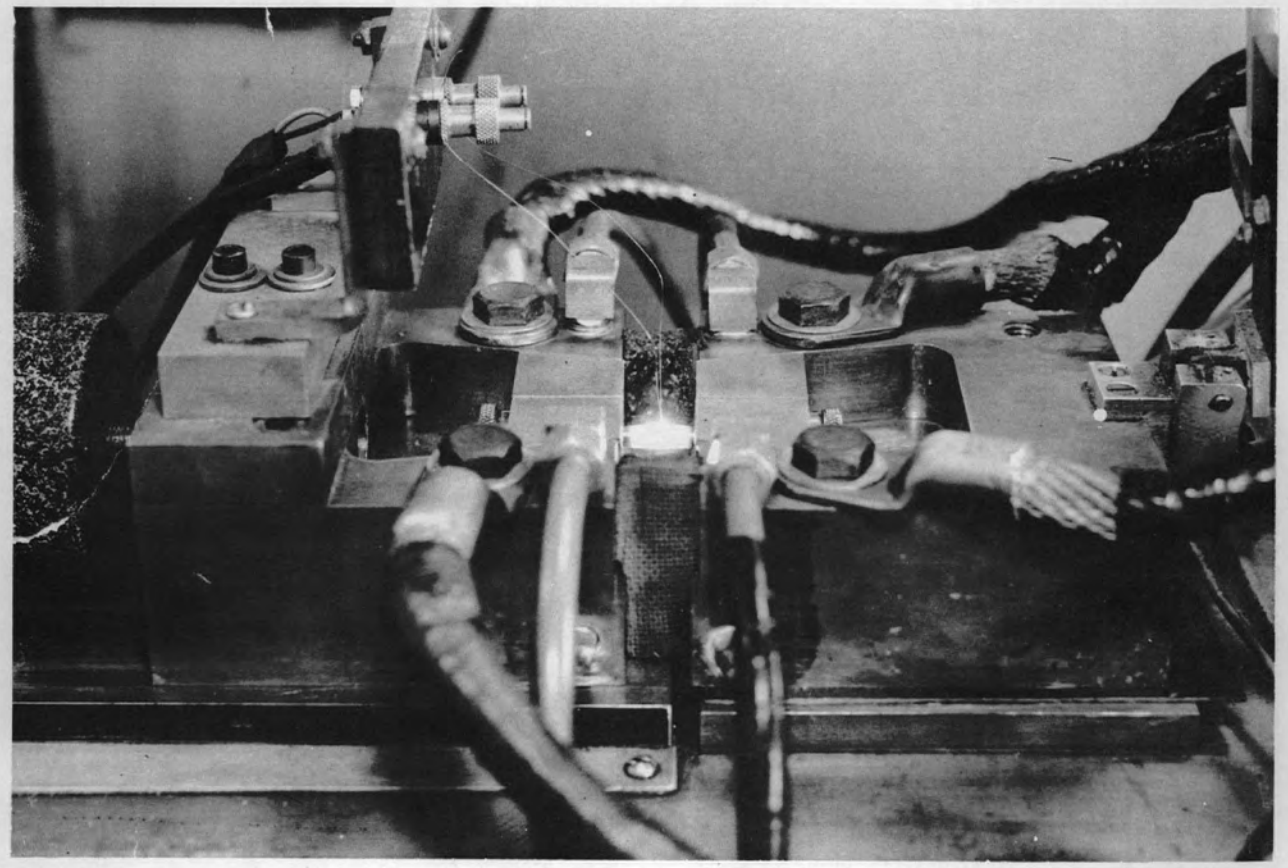

Fig. 8
Photograph of Test Specimen in Midst of an Actual Run

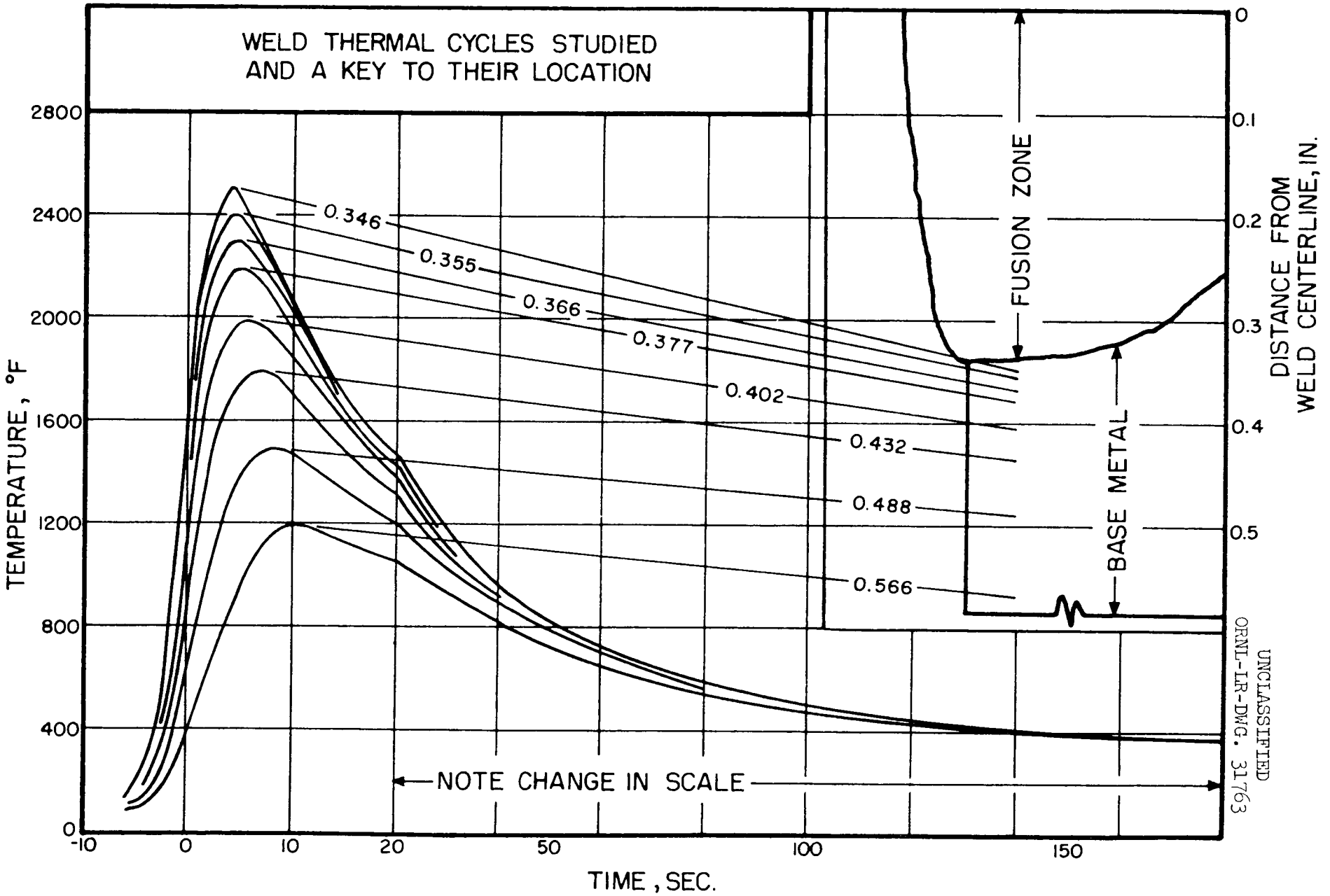

UNCLASSIFIED
ORNL-LR-DWG. 31763

FIG. 9

position of the resistor box was equivalent to a certain load as determined from the curve of load versus galvanometer deflection.

Thereafter, recalibration could be conveniently made by obtaining a record of the galvanometer deflections caused by the resistor box switch settings and plotting the deflections versus the known load equivalent of each switch setting.

Temperature Galvanometer

Calibration of the temperature galvanometer was accomplished by calibrating a battery box with a Brown potentiometer, each switch position on the box producing a millivoltage signal. Using a table for chromel-alumel thermocouples, these millivoltage signals were converted to degrees Fahrenheit. The battery box was then attached to the thermocouple terminals on the hot-ductility apparatus and an oscillographic trace made of the galvanometer deflections caused by each of the switch resistor positions of the battery box. This enabled the plotting of a calibration curve of temperature versus galvanometer deflection.

Strain Galvanometer

The strain galvanometer was calibrated by obtaining oscillographic traces of the galvanometer deflection with the probe in different positions, the probe movement corresponding to linear movement of the movable jaw.

To accomplish this, the probe was disconnected from the ram of the hydraulic piston. The probe was then advanced known increments of distance by the use of a micrometer depth gage clamped to the base of the hot-ductility apparatus, a trace of galvanometer deflection being made for every increment. A calibration curve was then plotted of probe movement versus galvanometer deflection.

Reduction-in-Area Data

To evaluate the ductility of specimens, the reduction-in-area at the fracture surface was measured. Each half of a specimen was measured twice, the readings taken at approximately right angles to each other, using a

graduated eyepiece. These four readings were then averaged to obtain a representative value.

Oscillographic Records

From the oscillographic traces, the deflections of the galvanometers were measured and converted by the use of calibration curves into maximum load to rupture, breaking temperature, and total strain.

Sensitivity of Measurements

Repeated checks of the various measurements indicated the following:

1. Reduction-in-area measurements were reproducible within 2%.
2. Load measurements were reproducible within 20 lb.
3. Strain measurements were reproducible within 0.05 in.

Review of Data

Upon completion of the testing program, all data were assembled and reviewed for possible bad tests. Such evaluations of the test was based on the Brush record of the current pulses during the cycle for each specimen, the recorded breaking temperature, the presence of fusion in the fracture, and the location of the thermocouple with respect to the fracture.

PART VI

RESULTS

Introduction

High-temperature properties obtained from tests on Hastelloy B specimens are presented in Tables III through VI. Figures 10 through 21 present these data in graphical form. Each point on the graphs represents an average of at least three tests, except where noted in the tables. The spread of experimental values at each testing temperature is indicated by the vertical bars. Where no vertical bar is shown, the experimental spread is covered by the circle representing the average value. The average strain rate of all tests is 1.0 in./sec.

Reduction-In-Area Data

Figure 10 summarizes the results of heating specimens to the indicated testing temperature and fracturing them.

The ductility of Hastelloy B is seen to increase slightly with testing temperature from 1500 to 2250°F. At 2300°F, the ductility has decreased markedly, and at 2350 and 2400°F the material is brittle.

The effect of a maximum temperature of 2400°F on the ductility of samples tested during the cooling portion of the cycle is shown in Figure 11. Between 1500 and 2000°F, there is little change in ductility. Above 2000°F, the ductility of the material decreases rapidly.

In Figure 12, the effect of a maximum temperature of 2350°F on the ductility of samples tested during cooling is shown. Here the ductility increases slightly with testing temperature up to 2200°F. Above 2200°F, the material is again embrittled.

Figure 13 shows results of samples subjected to a maximum temperature of 2300°F and fractured during the cooling portion of the cycle. The curve is similar to that of Figure 12.

TABLE III

RESULTS OF TESTS ON HASTELLOY B SAMPLES FRACTURED AT THE INDICATED TEMPERATURES DURING THE HEATING CYCLE

Testing Temperature (°F)	Reduction in Area (per cent)	Ave.	Ultimate Tensile Strength (psi)	Ave.	Total Strain (inches)	Ave.
2400	0.0	0.6	0	0	-	-
2400	0.0		0		-	-
2400	1.8		0		-	-
2350	1.6	1.2	9,270	11,900	0.025	0.025
2350	1.6		16,700		0.028	
2350	1.2		12,700		0.033	
2350	0.5		8,750		0.014	
2300	2.2	16.6	25,500	31,600	0.032	0.075
2300	4.7		29,600		0.038	
2300	5.0		30,600		0.073	
2300	1.2		23,600		0.038	
2300	26.2		31,300		0.100	
2300	14.3		31,300		0.074	
2300	30.0		-		0.033	
2300	27.8		38,000		0.108	
2300	31.0		37,700		0.126	
2300	21.7		37,200		0.115	
2300	18.8		-		0.088	
2250	41.1	41.8*	42,000	41,900*	0.156	0.154*
2250	42.5		41,800		0.152	
2200	42.6	39.8	43,800	42,400	0.144	0.145
2200	39.4		43,200		0.143	
2200	44.2		42,400		0.153	
2200	37.1		40,800		0.140	
2200	34.4		44,300		0.129	
2200	36.5		42,800		0.132	
2200	38.5		41,800		0.145	
2200	38.6		39,200		0.154	
2200	38.2		42,800		0.148	

* Denotes average of less than three tests

TABLE III (Cont'd)

Testing Temperature (°F)	Reduction in Area (per cent)	Ave.	Ultimate Tensile Strength (psi)	Ave.	Total Strain (inches)	Ave.
2000	37.8	35.9	-	56,400	0.189	0.194
2000	33.3		-		0.186	
2000	36.8		-		0.184	
2000	37.0		55,000		0.196	
2000	36.0		54,500		0.232	
2000	37.4		57,000		0.197	
2000	31.6		58,100		0.170	
2000	32.3		58,500		0.162	
2000	32.7		60,100		0.170	
1800	44.8	36.5	72,700	75,200	0.313	0.283
1800	33.7		76,700		0.240	
1800	37.4		76,700		-	
1800	34.7		76,400		0.294	
1800	33.0		74,800		0.278	
1800	35.5		73,900		0.290	
1500	24.2	27.0	-	89,000	-	0.420*
1500	23.4		-		-	
1500	27.5		-		-	
1500	27.0		90,800		0.417	
1500	22.6		90,800		0.423	
1500	20.9		88,400		-	
1500	34.4		-		-	
1500	32.5		88,100		-	
1500	30.1		87,100		-	

* Denotes average of less than three tests

TABLE IV

RESULTS OF TESTS ON HASTELLOY B SAMPLES
HEATED TO 2400°F AND FRACTURED AT THE INDICATED
TEMPERATURES DURING THE COOLING CYCLE

Testing Temperature (°F)	Reduction in Area (per cent)	Ave.	Ultimate Tensile Strength (psi)	Ave.	Total Strain (inches)	Ave.
2300	0.9	2.4	131	20,400	-	0.036
2300	0.0		8,180		-	
2300	4.0		25,800		-	
2300	2.9		31,800		0.036	
2300	2.9		28,600		0.036	
2300	3.2		26,500		0.036	
2200	19.2	14.6	7,680	21,800	-	0.075
2200	11.1		7,340		-	
2200	6.1		7,340		-	
2200	33.8		32,200		0.128	
2200	34.2		32,200		0.128	
2200	6.9		-		-	
2200	7.0		38,900		0.038	
2200	5.8		37,000		0.050	
2200	7.4		34,600		0.033	
2000	39.4	33.9	42,400	49,900	-	0.193
2000	38.6		45,400		-	
2000	36.1		43,900		-	
2000	32.8		-		0.213	
2000	34.5		-		0.218	
2000	28.8		55,500		0.188	
2000	30.2		56,100		0.165	
2000	30.8		56,100		0.179	
1800	24.2	27.6	64,600	67,000	-	0.295
1800	25.2		66,100		-	
1800	27.8		67,600		-	
1800	28.5		68,800		0.290	
1800	30.4		67,300		0.280	
1800	30.0		67,300		0.316	
1500	24.4	29.7	-	80,200*	-	0.280*
1500	26.5		-		-	
1500	24.1		-		-	
1500	24.4		79,700		-	
1500	25.6		80,800		0.280	

* Denotes average of less than three years

TABLE IV (Cont'd)

Testing Temperature (°F)	Reduction in Area (per cent) Ave.	Ultimate Tensile Strength (psi) Ave.	Total Strain (inches) Ave.
1500	35.2	-	-
1500	36.9	-	-
1500	36.2	-	-
1500	34.5	-	-
1500	33.4	-	-
1500	35.5	-	-

* Denotes average of less than three tests

TABLE V

RESULTS OF TESTS ON HASTELLOY B SAMPLES
HEATED TO 2350°F AND FRACTURED AT THE INDICATED
TEMPERATURES DURING THE COOLING CYCLE

Testing Temperature (°F)	Reduction in Area (per cent)	Ave.	Ultimate Tensile Strength (psi)	Ave.	Total Strain (inches)	Ave.
2300	2.7	5.0	21,600	28,600	0.028	0.030
2300	7.3		41,200		0.033	
2300	5.0		23,000		0.030	
2200	40.6	41.2	42,800	43,600	0.126	0.137
2200	41.2		44,800		0.138	
2200	41.8		43,200		0.148	
2000	33.0	34.2*	53,500	55,200*	0.160	0.195*
2000	35.5		57,000		0.230	
1800	30.0	31.1	70,800	70,700	0.317	0.320
1800	31.7		71,400		0.332	
1800	31.5		70,000		0.312	

* Denotes average of less than three tests

TABLE VI

RESULTS OF TESTS ON HASTELLOY B SAMPLES HEATED TO 2300°F AND FRACTURED AT THE INDICATED TEMPERATURES DURING THE COOLING CYCLE

Testing Temperature (°F)	Reduction in Area (per cent)	Ave.	Ultimate Tensile Strength (psi)	Ave.	Total Strain (inches)	Ave.
2200	40.9	38.1	43,200	41,900	0.133	0.136
2200	41.6		43,100		0.132	
2200	40.6		43,500		0.138	
2200	33.4		39,800		0.131	
2200	36.5		41,300		0.143	
2200	35.4		40,300		0.140	
2000	33.7	33.2	-	56,200	0.188	0.192
2000	35.6		-		0.220	
2000	37.8		-		0.215	
2000	31.0		57,100		0.179	
2000	30.8		55,500		0.174	
2000	30.2		56,100		0.174	
1800	32.5	32.7	71,700	70,600	0.270	0.306
1800	32.2		69,900		0.356	
1800	33.5		70,200		0.292	

UNCLASSIFIED
ORNL-LR-DWG. 31764

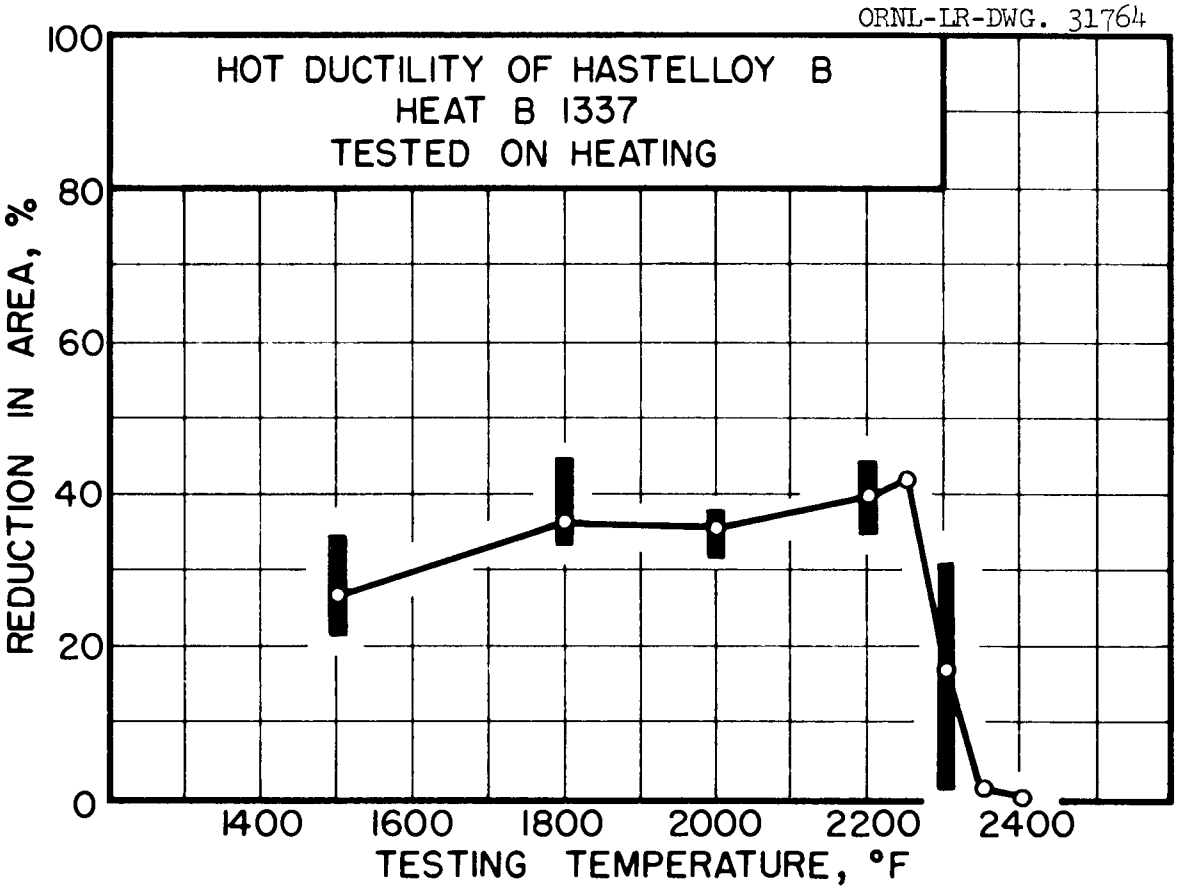

FIG. 10

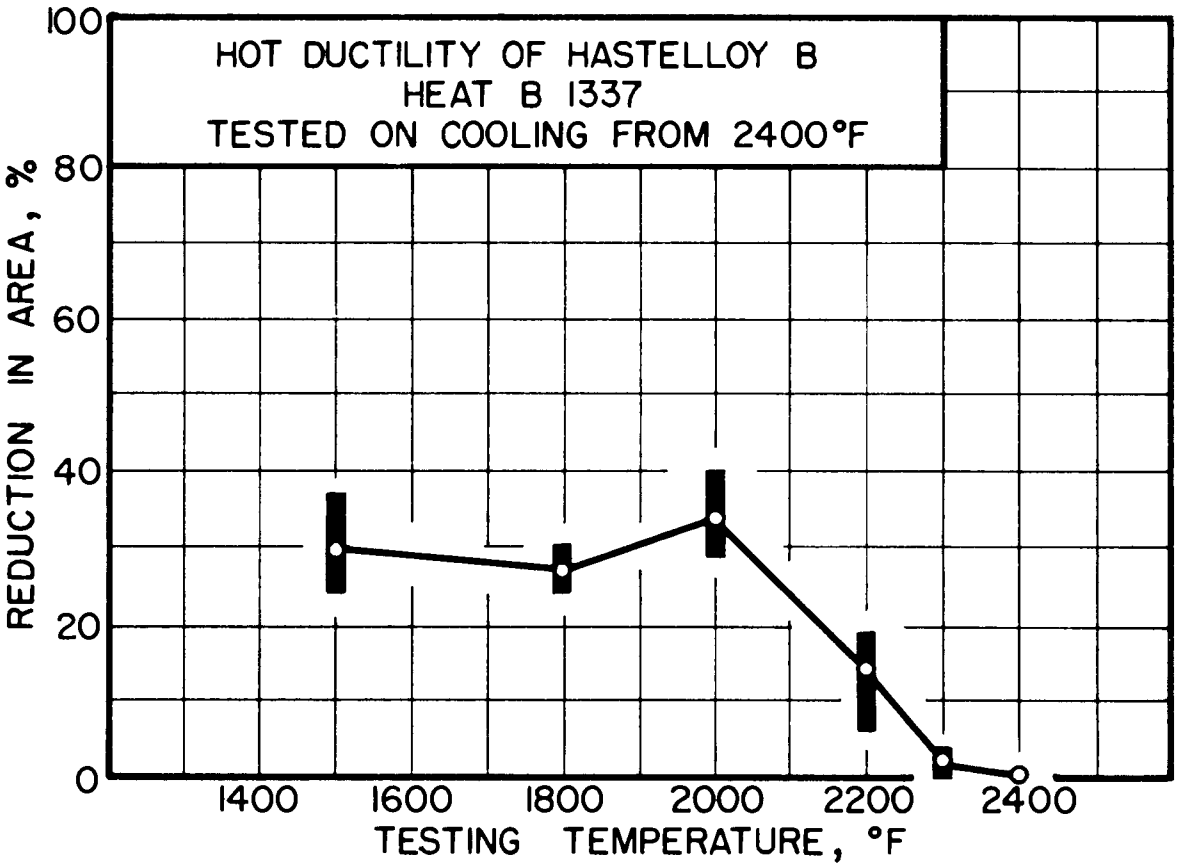

FIG. 11

UNCLASSIFIED
ORNL-LR-DWG. 31765

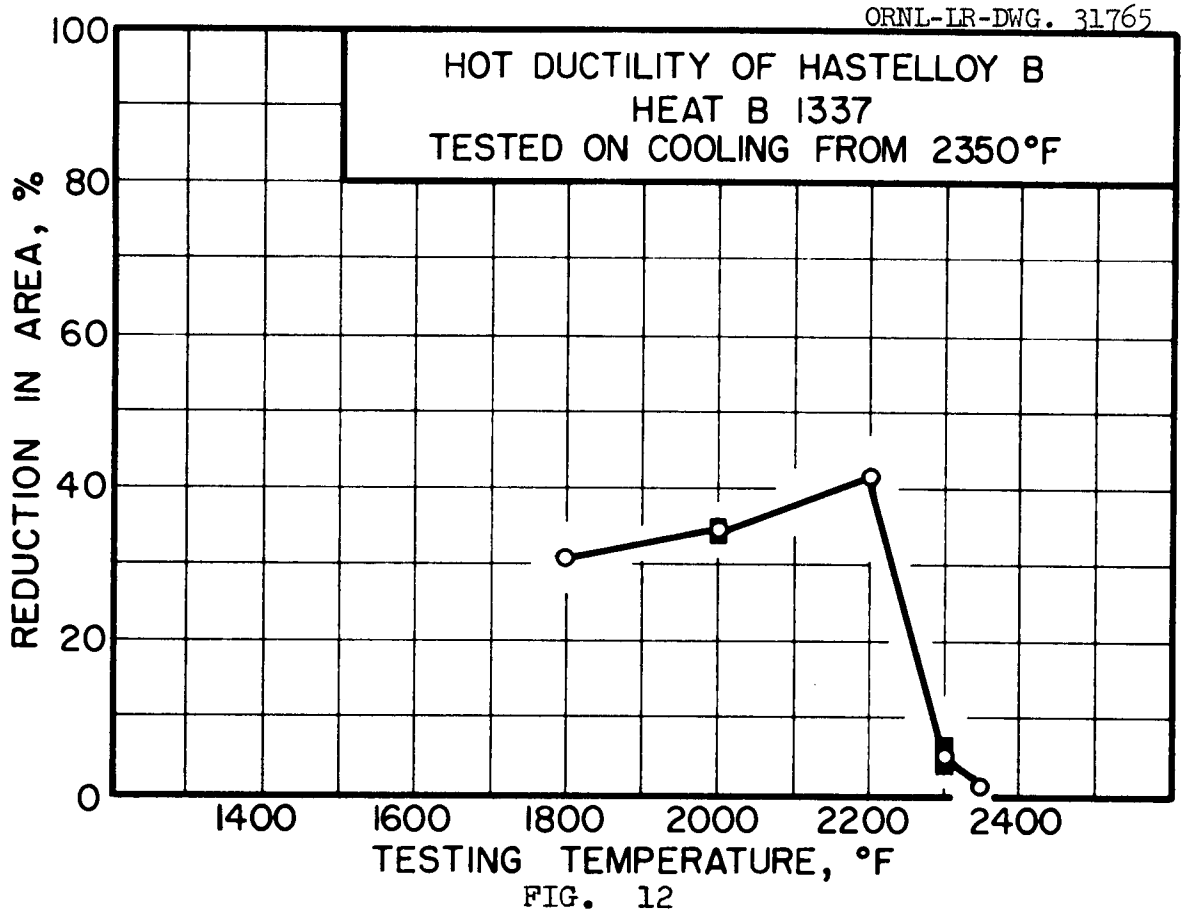

FIG. 12

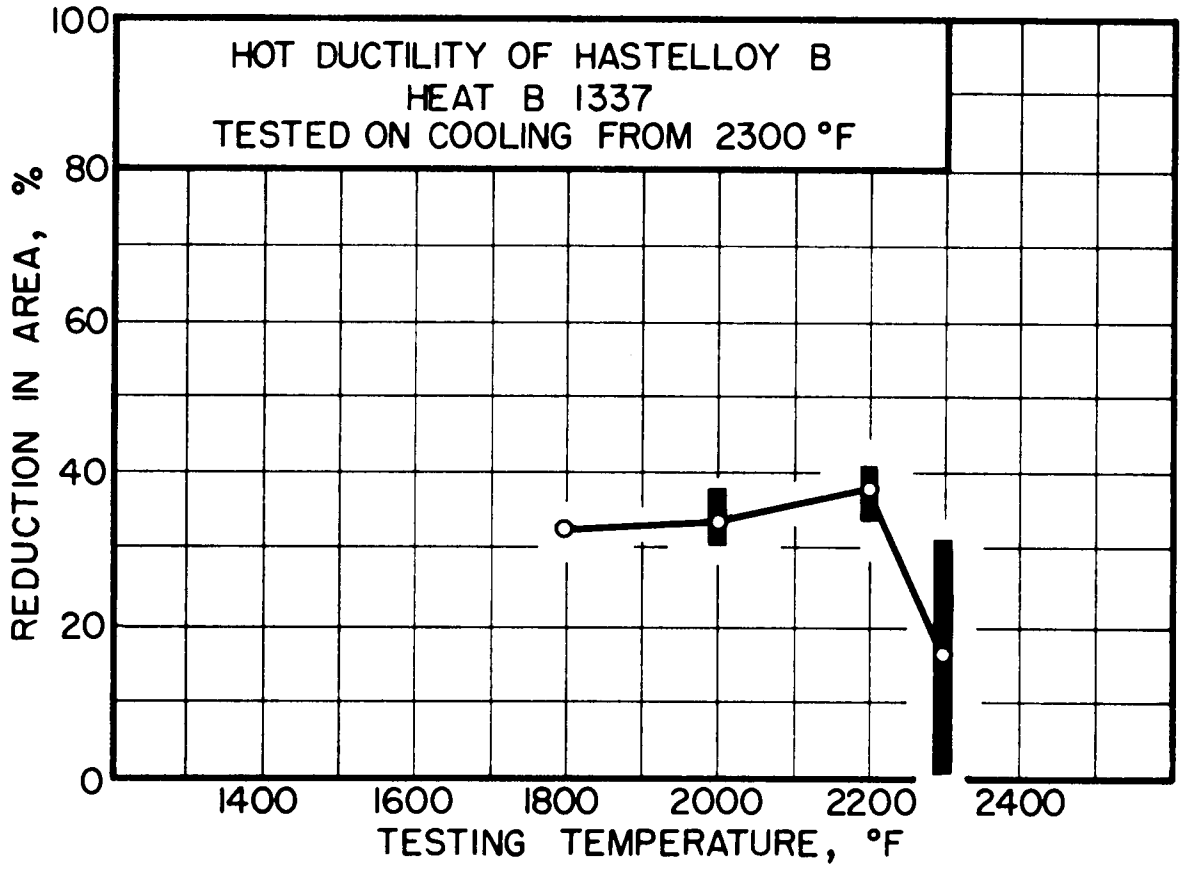

FIG. 13

UNCLASSIFIED
ORNL-LR-DWG. 31766

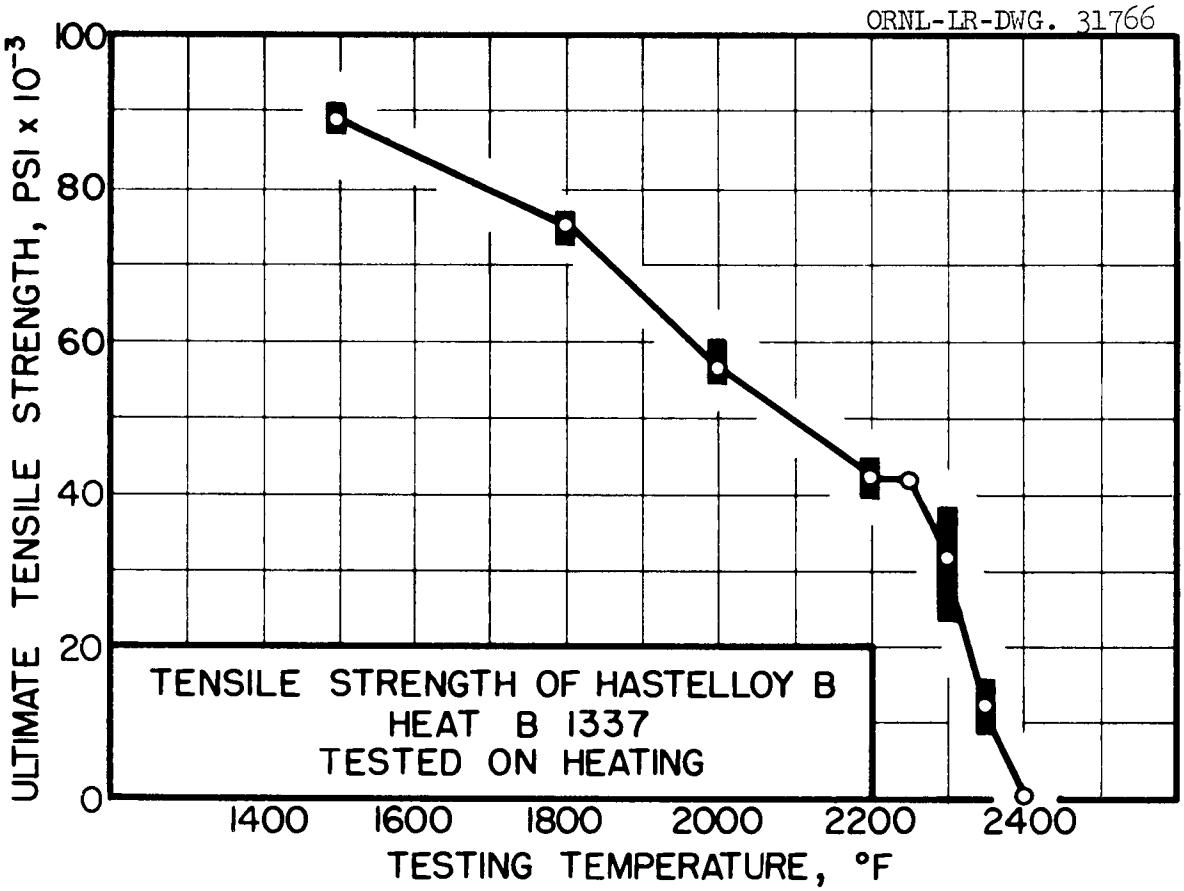

FIG. 14

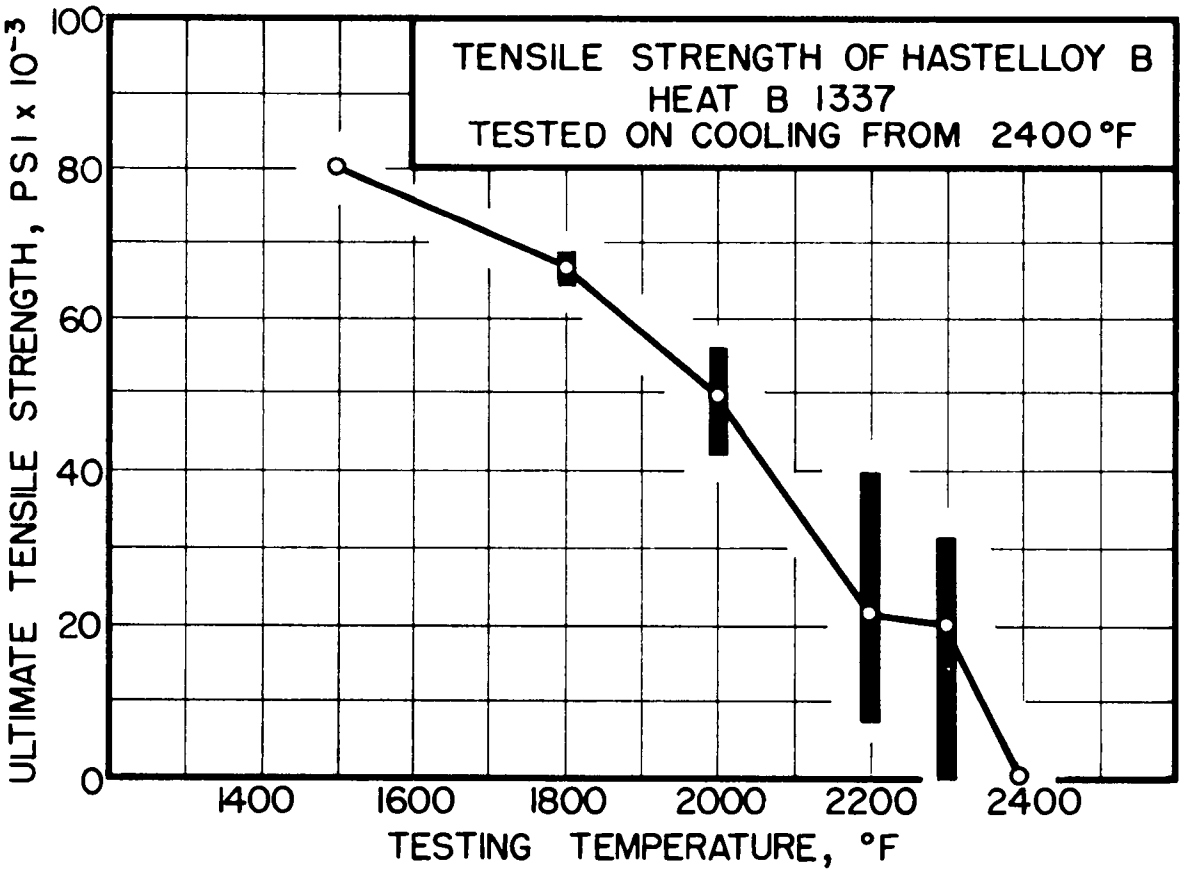

FIG. 15

UNCLASSIFIED
ORNL-LR-DWG. 31767

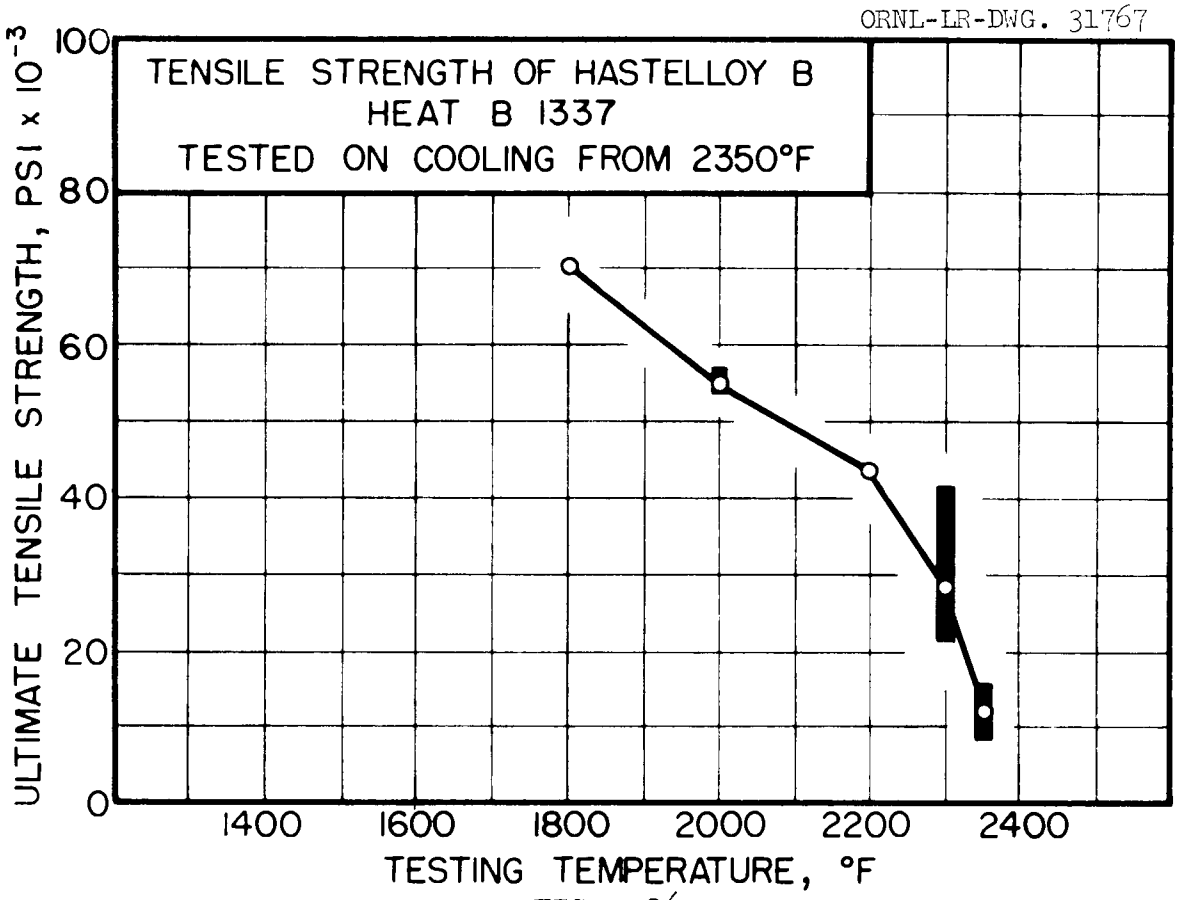

FIG. 16

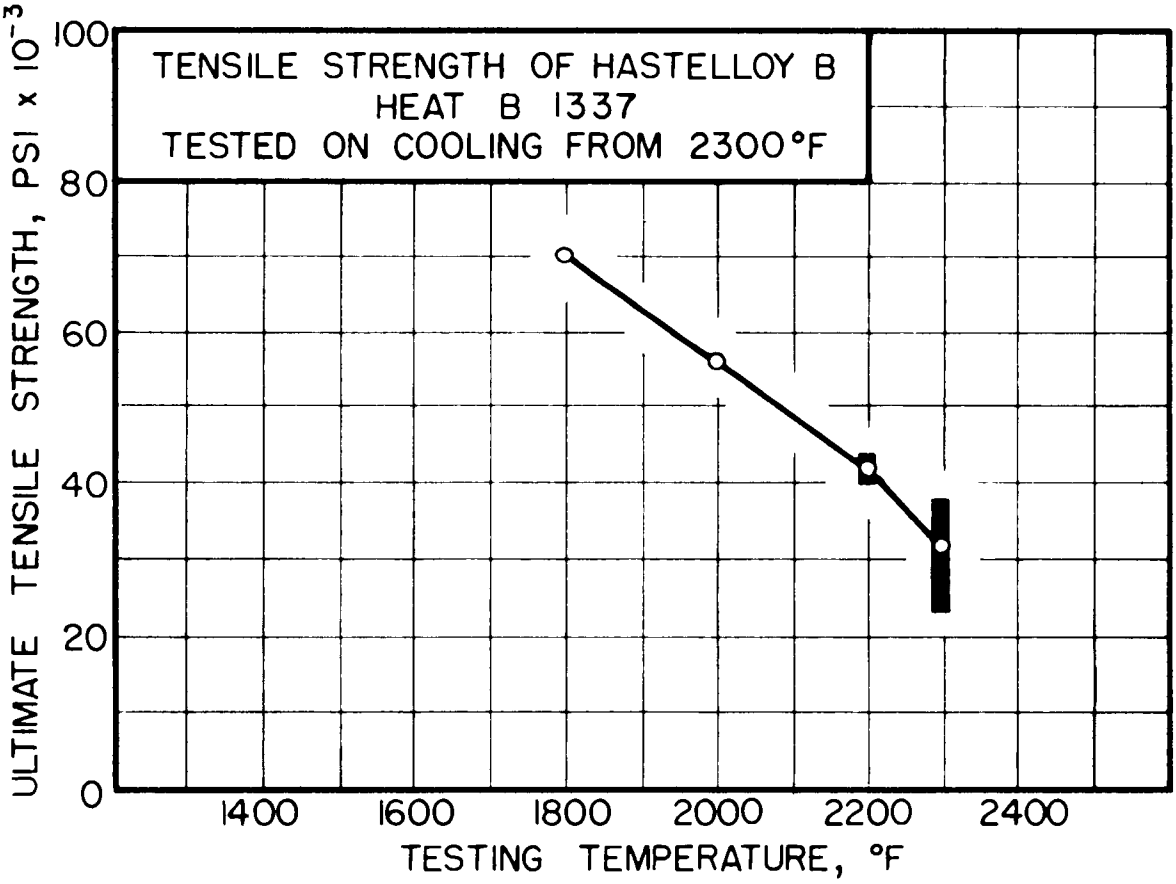

FIG. 17

UNCLASSIFIED
ORNL-LR-DWG. 31768

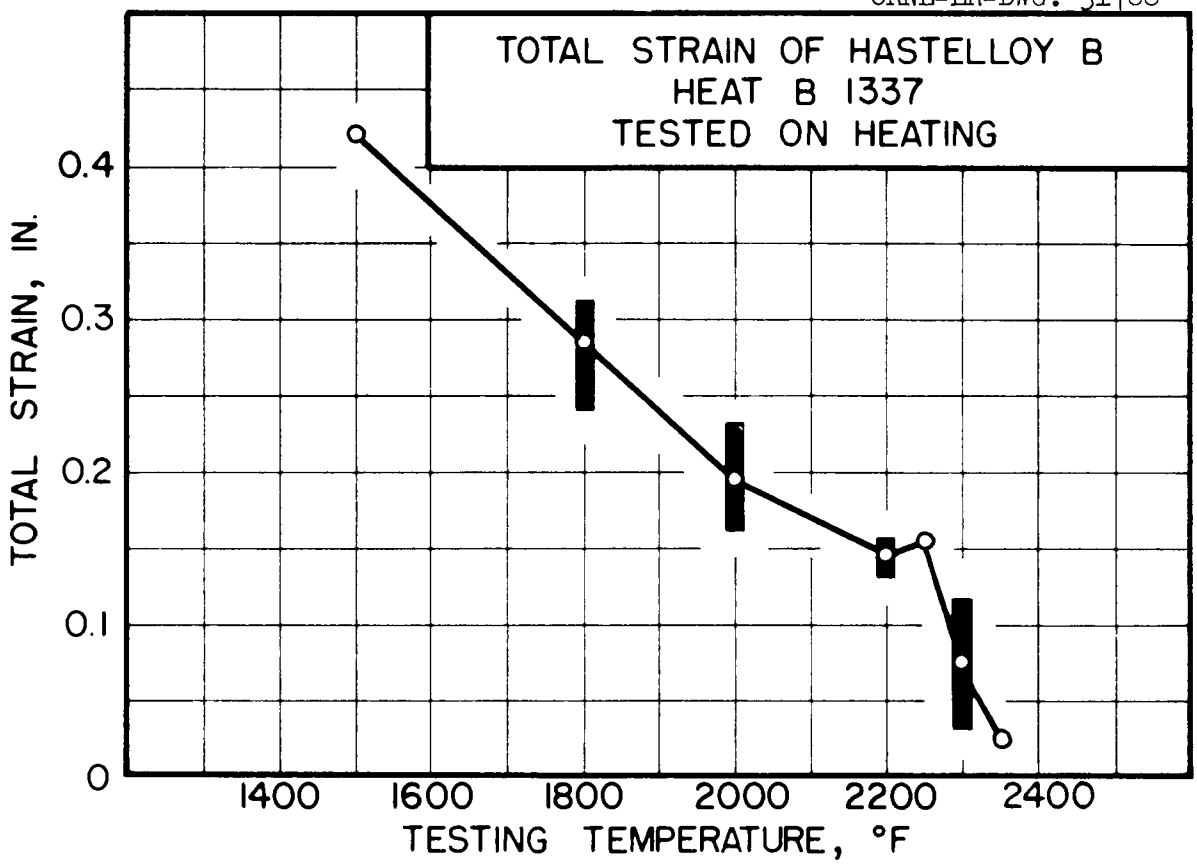

FIG. 18

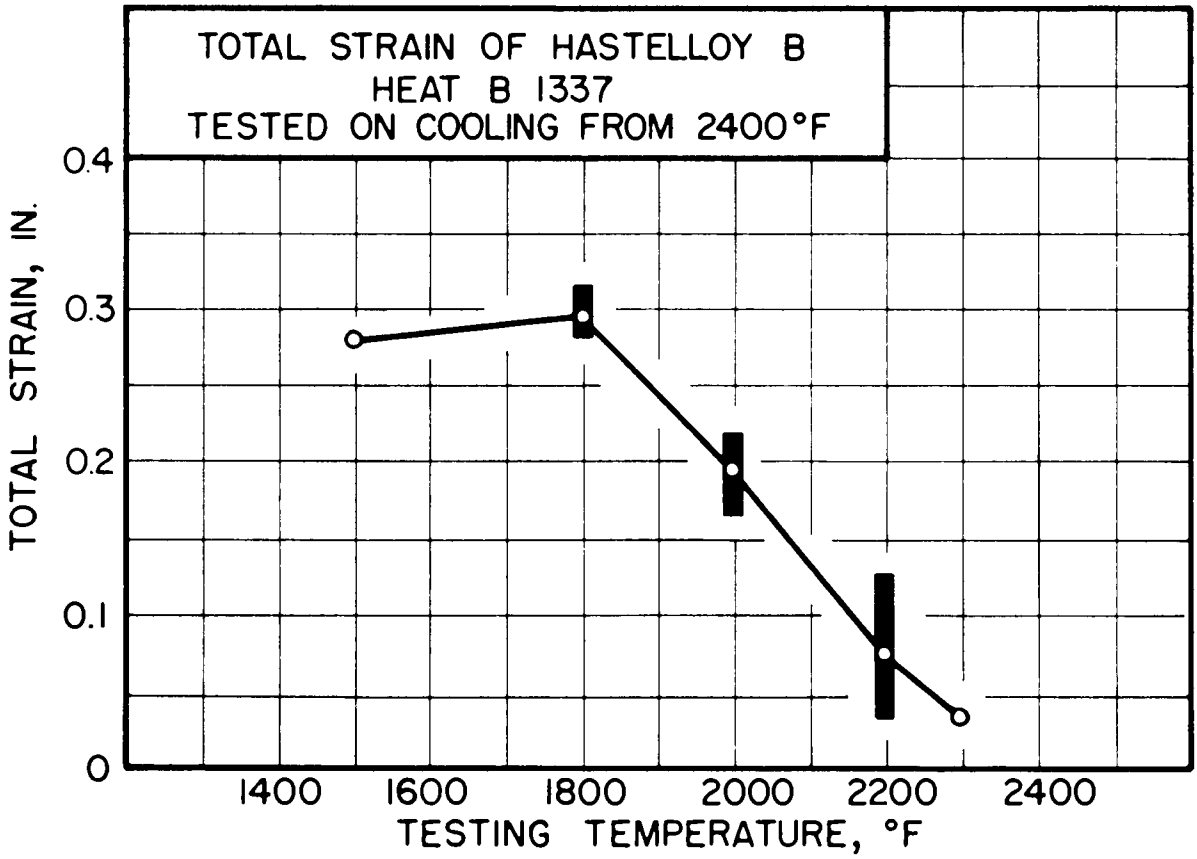

FIG. 19

UNCLASSIFIED
ORNL-LR-DWG. 31769

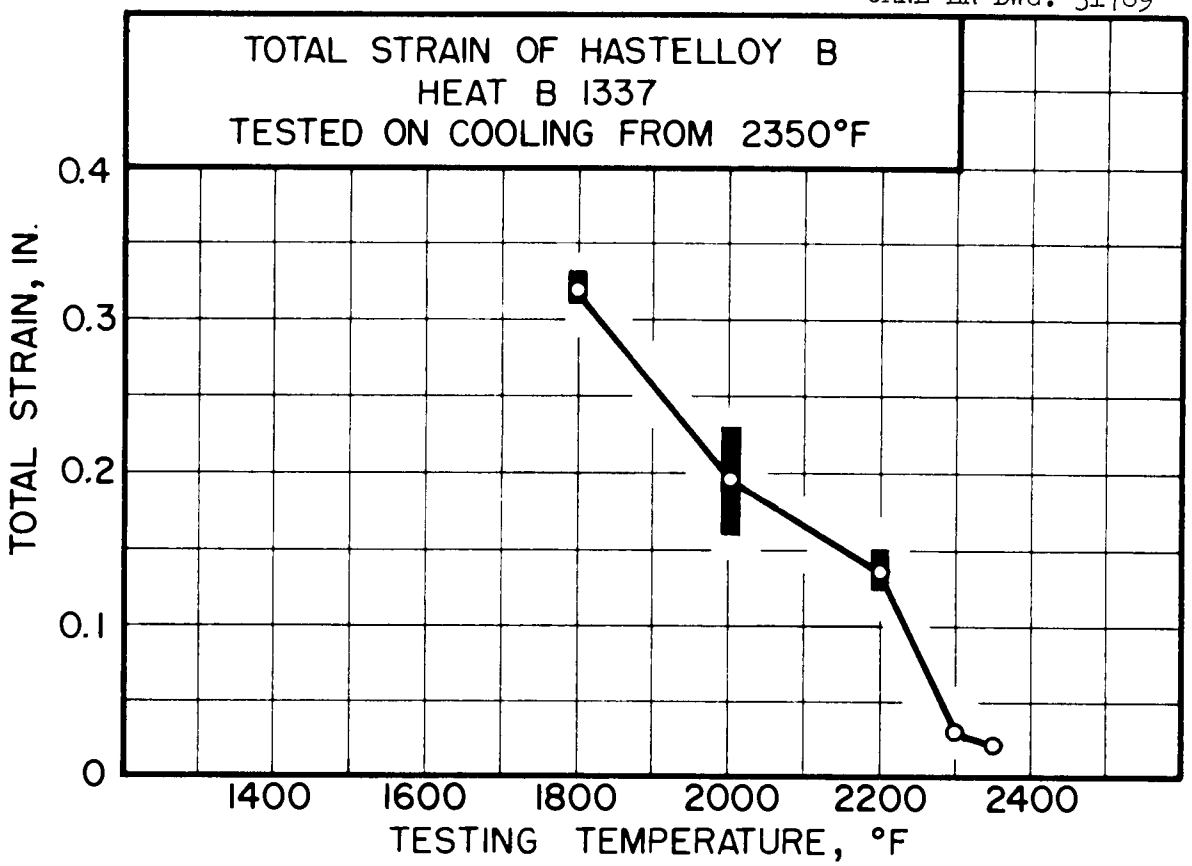

FIG. 20

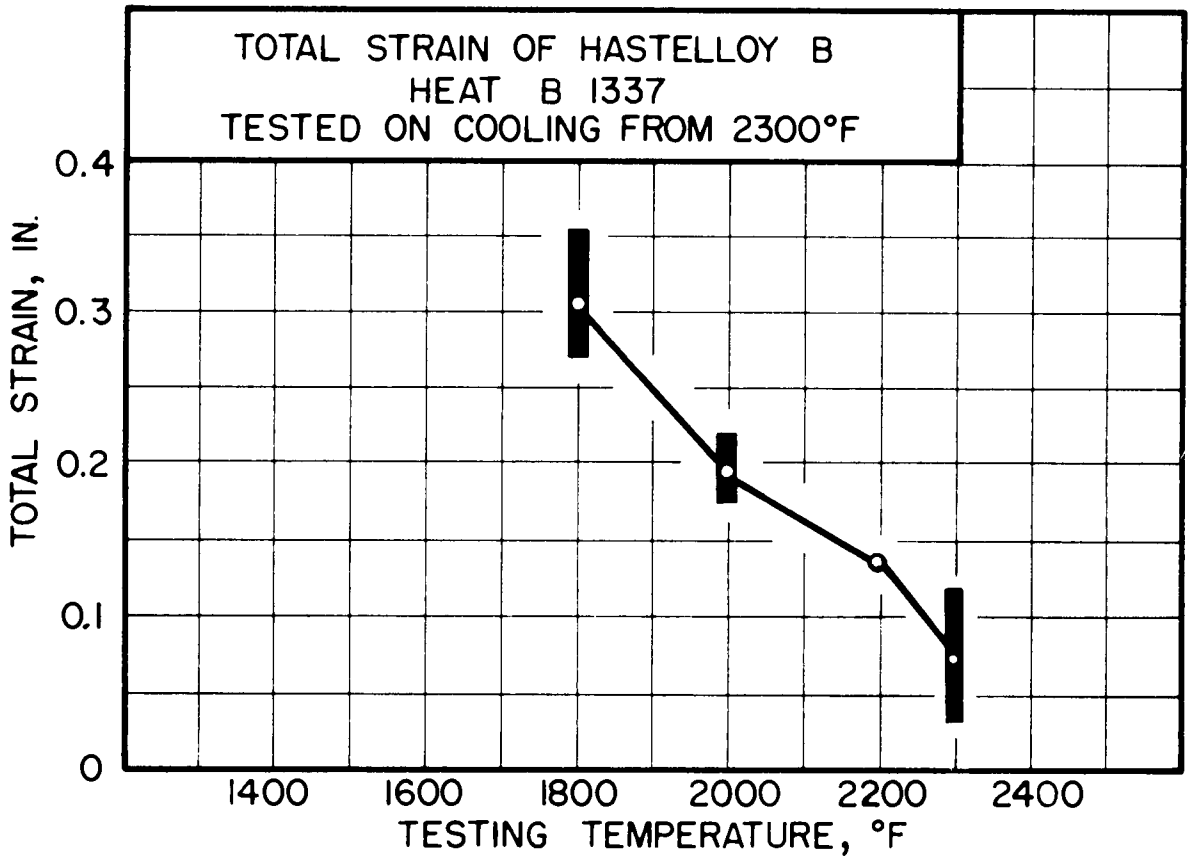

FIG. 21

From these reduction-in-area graphs, two points of significance should be noted:

1. In all cases, the material loses ductility at high testing temperatures.
2. Even more important, the severity of impairment of ductility at these high testing temperatures (as compared with results for samples tested on heating) increases as the maximum temperature to which the material was subjected increases.

Tensile-Strength Data

Figures 14, 15, 16, and 17 are graphical representations of the variation in tensile strength with thermal cycles. In all cases, the curves are generally of the shape that would be expected; that is, the tensile strength decreasing continuously and along a smooth curve as testing temperature increases. Only two irregularities appear in these curves, one in Figure 14 at a testing temperature of 2250°F and one in Figure 15 at a temperature range of 2200°F to 2300°F.

Comparison of Figures 14 and 15 shows that those samples subjected to a 2400°F thermal cycle have less strength than the samples tested on heating. This effect is apparent at all testing temperatures and amounts to a loss of about 10,000 psi tensile strength.

Those samples subjected to thermal cycles of 2350 and 2300°F (Figures 16 and 17) evince no loss in tensile strength when compared to samples tested on heating.

Strain Data

Generally speaking, the curves of Figures 18, 19, 20, and 21 summarizing the strain data resemble those tensile curves which are their counterparts. That is, there is a decrease in total strain as the testing temperature increases, regardless of the thermal cycle involved. The only exception to this observation is the strain value for the 1500°F testing temperature of Figure 18. This would be considered an anomaly

were it not for the fact that this point represents a single test result and not an average of several tests.

Comparing the average values of test results for total strain, it is interesting to note that for all cases where samples were fractured on the cooling portion of their respective thermal cycles, at those temperatures at which ductility was lost as compared with test results on heating, so also was there some loss in total strain. However, this loss is not considered significant, since the spreads of measured values at a single testing temperature overlap. For example, while a comparison of strain values of Figures 18 and 19 at a testing temperature of 2300°F show a difference of 0.03 in. in the average values, the minimum value of strain for Figure 18 and the maximum value for Figure 19 are both 0.04 in.

METALLOGRAPHIC OBSERVATIONS

A study was made of changes in the microstructure of Hastelloy B resulting from certain thermal cycles to which samples of the material had been subjected.

The structure of Hastelloy B in the as-received condition consisted of a nickel-rich solid solution (α) containing essentially a single secondary phase present in the globular form. The secondary phase has been reported by Monkman et al., as the intermetallic compound NiMo (δ). This structure was unchanged for samples tested at any temperature up to and including 2200°F. The photomicrograph of Figure 22 is typical of the appearance of this structure. In the as-polished condition, only the δ phase in the nickel-rich solid solution may be seen.

Figure 23 consists of photomicrographs of a sample heated to 2300°F and fractured. Discontinuous grain boundary films are present and are shown at low and high magnifications.

Figure 24 shows the structure resulting from heating a specimen to 2350°F and cooling to 2200°F before fracturing it. Again, the only change has been the formation of discontinuous grain boundary films, but comparison with Figure 23a reveals these films to be more prevalent than in the sample subjected to a maximum temperature of 2300°F.

UNCLASSIFIED
PHOTO 44567

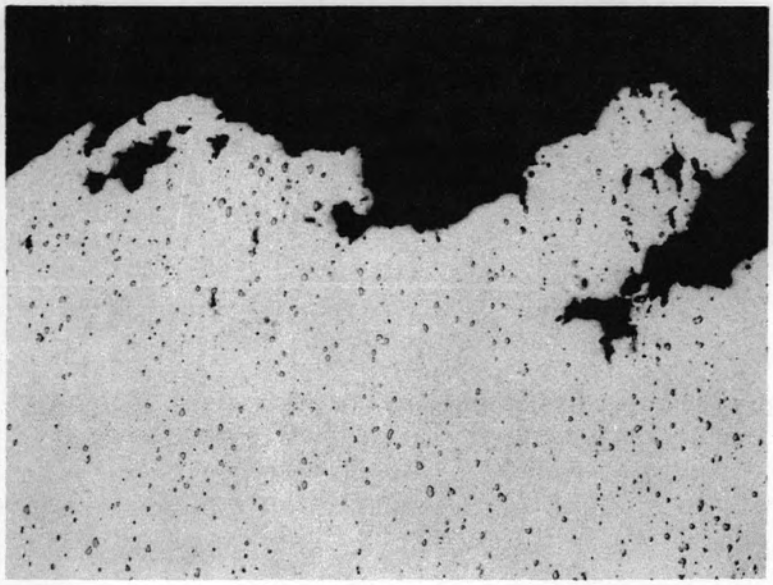

100X As Polished

Fig. 22

Microstructure of Hastelloy B Sample Fractured
At 2200°F on Heating

UNCLASSIFIED
PHOTO 44568

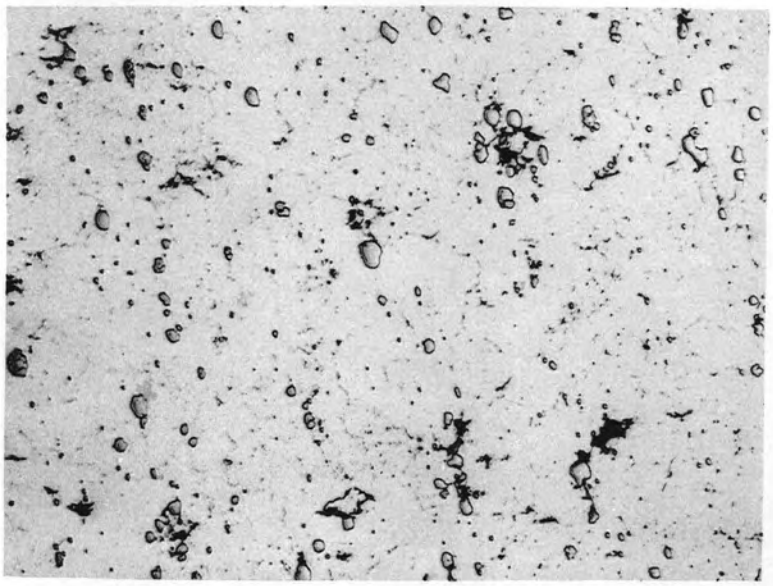

Fig. 23a 250X

Appearance of Grain-Boundary Films in Hastelloy B at Low Magnification

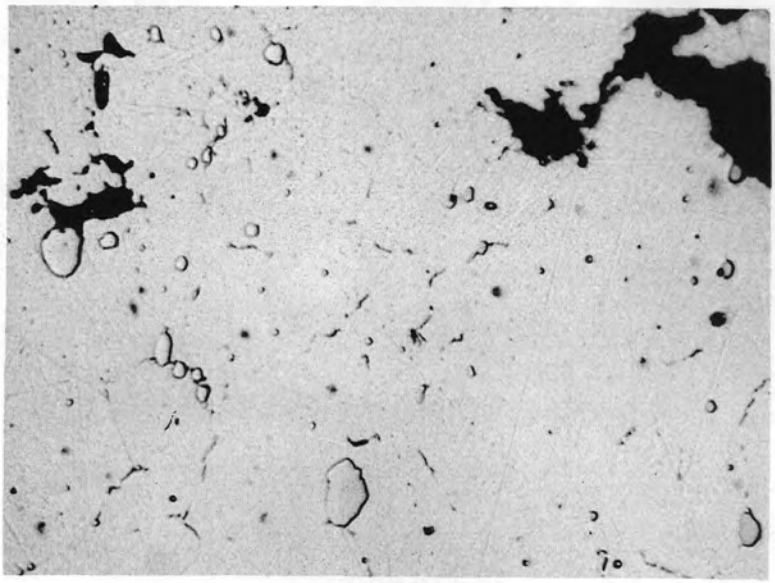

Fig. 23b 1000X

Appearance of Grain-Boundary Films in Hastelloy B at High Magnification

Fig. 23. Microstructure of Hastelloy B Sample Fractured at 2300°F on Heating (Etchant- 1:1:1 HCl, HNO_3, H_2O)

UNCLASSIFIED
PHOTO 44569

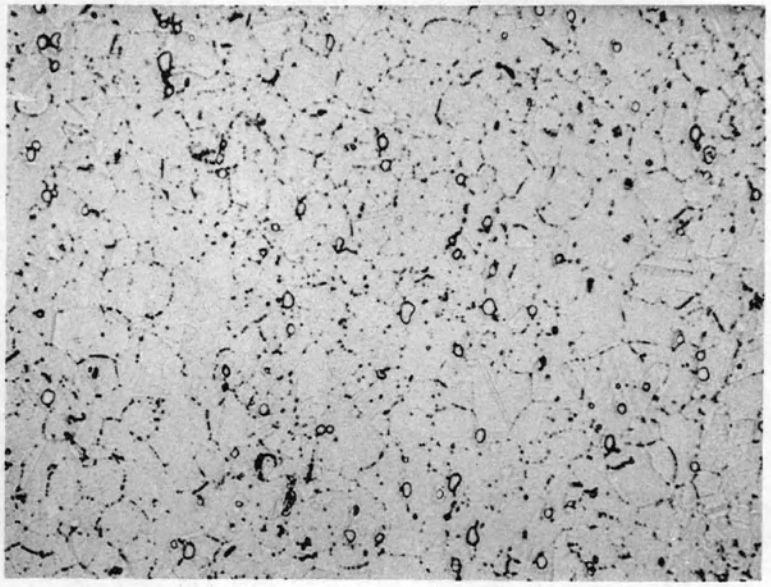

Fig. 24 250X

Microstructure of Hastelloy B Sample Fractured at 2200°F on Cooling from 2350°F (Etchant- 1:1:1 HCl, HNO_3, H_2O)

Subjecting a Hastelloy B sample to a thermal cycle having a peak temperature of 2400°F causes a striking change in microstructure. As the survey of Figure 25 shows, a transition in structure occurs as the sample is traversed from the base material to the fracture surface. Figure 25a is essentially the as-received structure unaffected by heat. Figure 25b is a photomicrograph of the transition zone which has been somewhat affected by heat treatment. In this zone it may be seen that the δ phase is breaking up and redistributing itself primarily along the grain boundaries of the material. On redistributing, the grain boundary constituent has an appearance commonly referred to as "Chinese script". Near the fracture surface of the specimen, the transition has been completed and appears as shown in Figure 25c.

This redistribution of the δ phase appears as two structures which are clearly differentiated at the higher magnification of Figure 26. These structures are caused by the thermal gradient in the specimen. The first structure is found in the transition zone, and the resulting material is the afore-mentioned "Chinese script". The second structure occurs at the higher temperature near the fracture surface of the specimen and is the eutectic structure of Figure 26b. Note that this eutectic is associated with grain-boundary melting which occurred in this specimen.

The microstructure of a sample fractured at 2300°F on cooling from 2400°F is identical in appearance to the sample fractured at 2400°F. In such a sample, the eutectic at low magnification appears as in Figure 27a. The transition zone in this sample appears as in Figure 27b.

In an attempt to learn more about the structural changes in the temperature range of 2250°F to 2400°F, four samples were subjected to the thermal cycles listed below, using the time-temperature controller.

1. Heated to 2400°F, held for 2 min at temperature, cooled rapidly to room temperature.
2. Heated to 2350°F, held for 5 min at temperature, cooled rapidly to room temperature.
3. Heated to 2300°F, held for 5 min at temperature, cooled rapidly to room temperature.
4. Heated to 2250°F, held for 5 min at temperature, cooled rapidly to room temperature.

UNCLASSIFIED
PHOTO 44570

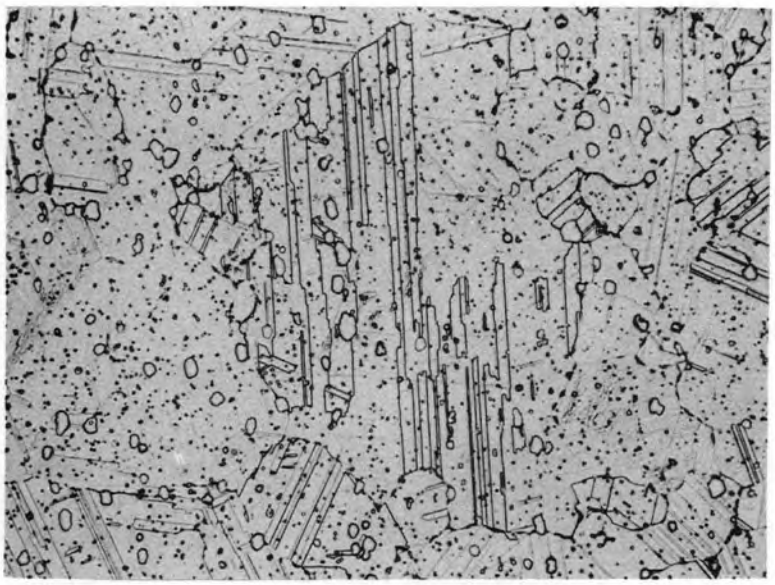

Fig. 25a 250X

Microstructure of Unaffected Base Material

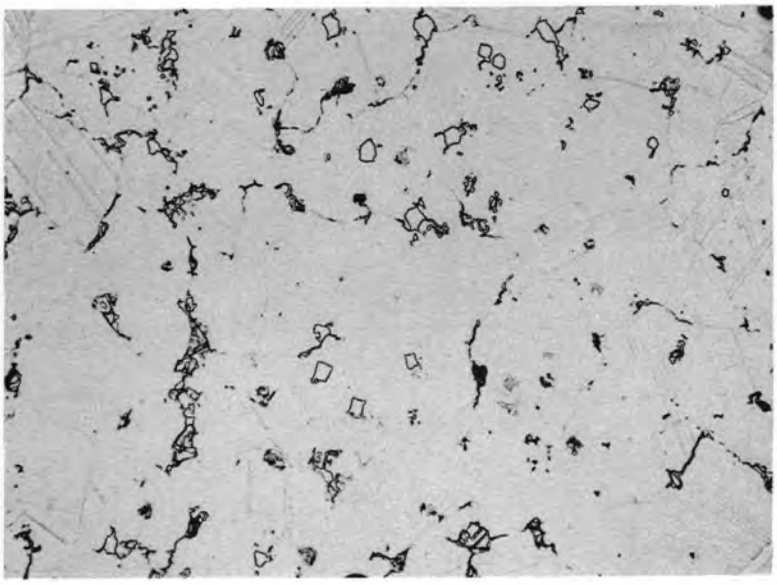

Fig. 25b 250X

Microstructure of Transition Area of Heat-Affected Zone

Fig. 25. Microstructural Changes Occurring in a Hastelloy B Sample Fractured at 2400°F on Heating (Etchant- 1:1:1 HCl, HNO_3, H_2O)

UNCLASSIFIED
PHOTO 44571

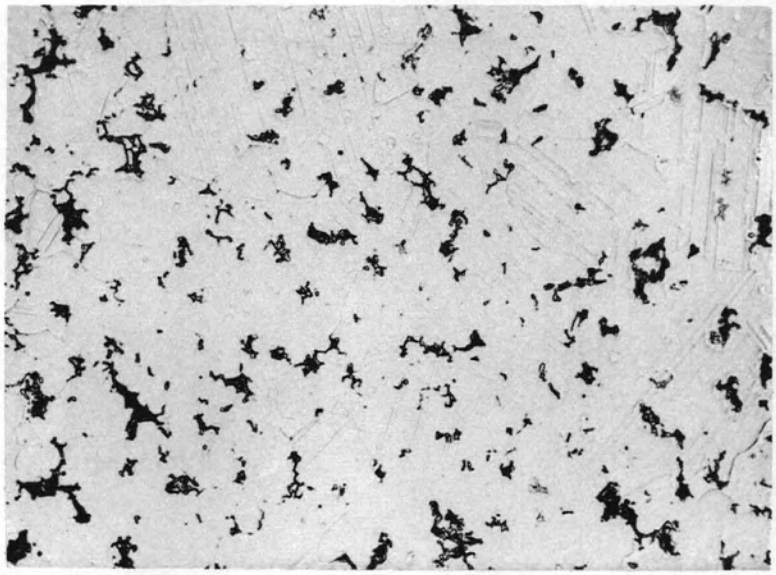

Fig. 25c 250X

Microstructure of Heat-Affected Zone Near Fracture Surface

Fig. 25. Microstructural Changes Occurring in a Hastelloy B Sample Fractured at 2400°F on Heating (Etchant- 1:1:1 HCl, HNO_3, H_2O)

UNCLASSIFIED
PHOTO 44572

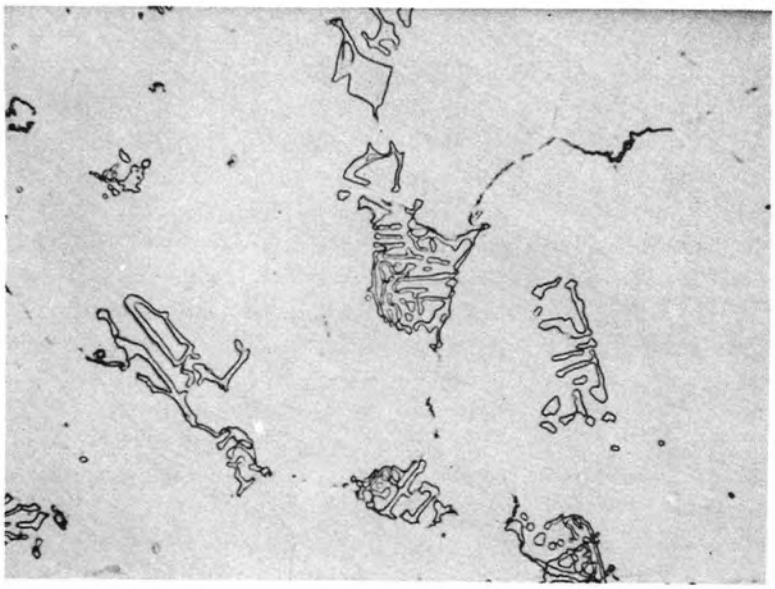

Fig. 26a 1000X

Appearance of Eutectic in Transition Zone

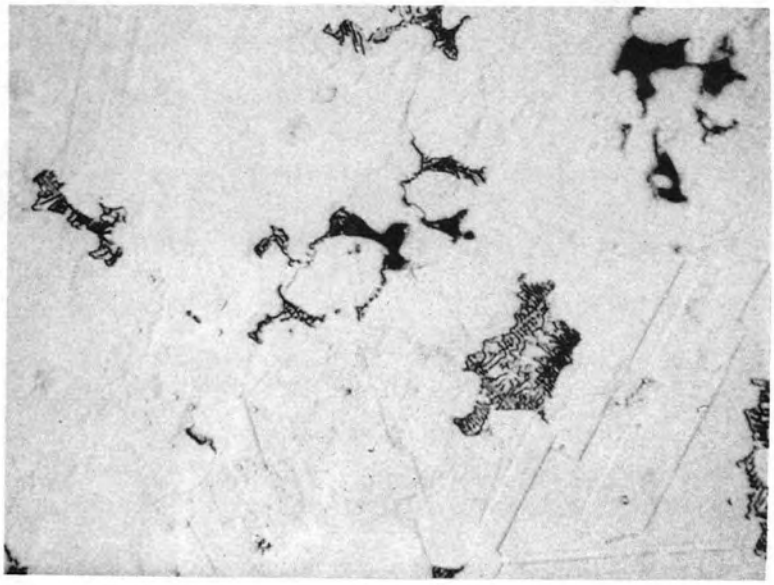

Fig. 26b 1000X

Appearance of Eutectic Near Fracture Surface

Fig. 26. Appearance of Eutectic at High Magnification
(Etchant- 1:1:1 HCl, HNO_3, H_2O)

UNCLASSIFIED
PHOTO 44573

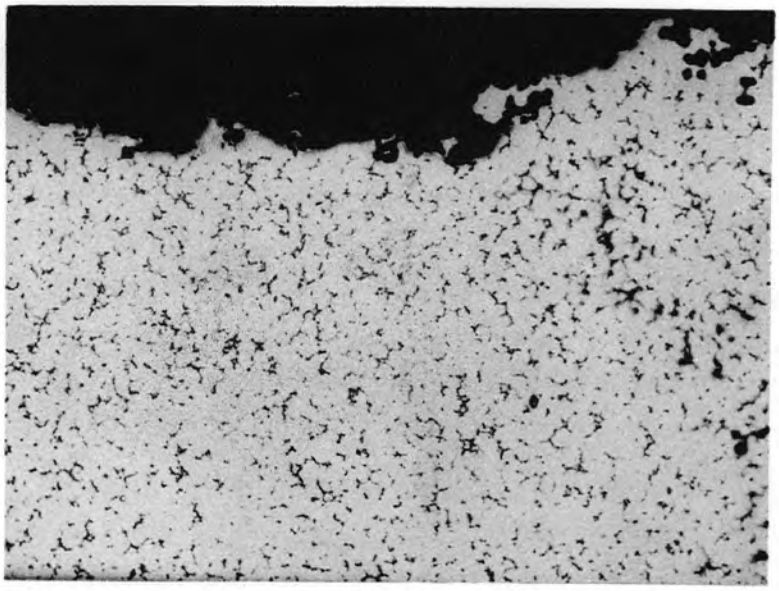

Fig. 27a 100X

Appearance of Eutectic at Low Magnification
(Fracture Surface at Top of Picture)

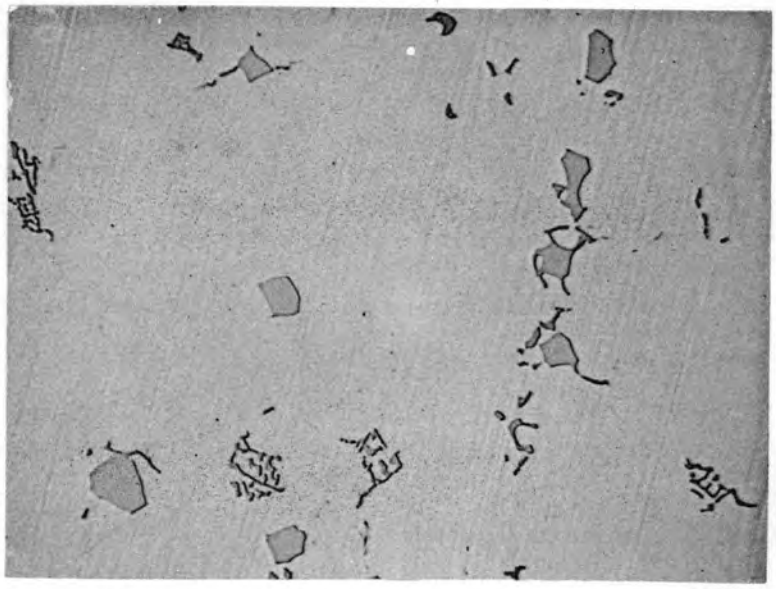

Fig. 27b 1000X

Appearance of Eutectic at High Magnification

Fig. 27. Microstructure of Hastelloy B Sample Fractured at 2300°F on Cooling from 2400°F (Etchant- 1:1:1 HCl, HNO_3, H_2O)

The heating rate for these samples was the same as that for samples subjected to 2400°F thermal cycles. The cooling rate for these samples was approximately 300°F/sec. All samples were protected during heat treatment with an argon atmosphere.

Some effects of these thermal cycles are shown in Figures 28, 29, 30, and 31. The sections selected for study were taken to show the effect of a thermal gradient on the microstructure of the material.

Figure 28a is a photomicrograph of the transition from the base material on the left through the heat-affected zone on the right for a 2250°F heat treatment. The effect produced has been a coarsening of the grain size throughout the heat-affected zone. No change in the distribution or appearance of the δ phase is noticeable. As shown in Figures 28b and 28c, there is a difference in the appearance of the grain boundaries of the base material and heat-affected zone. Whereas the base material had some grain-boundary constituent, the thermal treatment has caused the formation of a continuous grain-boundary film.

The 2300°F thermal cycle has resulted in the microstructure shown in Figure 29. This structure is very similar to Figure 28a, except that the grain size in the heat-affected zone is larger. Again, the base material is at the left of the photograph.

A study of the sample which was given the 2350°F thermal cycle showed a further increase in grain size through the heat-affected zone. Two additional effects were noted. As shown in Figure 30, the grain-boundary film had built up so that it was resolvable in some areas. Also, at the center of the heat-affected zone, some of the eutectic structure was found.

As in the samples subjected to the normal 2400°F thermal cycle, the most striking microstructural changes are produced in the sample heat treated for 2 min at this temperature. These microstructural changes are shown in Figure 31. At 50X, Figure 31a shows a transition zone where considerable solution of the δ phase has taken place. The grains in this zone are markedly coarsened. However, the center of the heat-affected zone on the right shows very little grain coarsening. Instead, the eutectic has formed at the grain boundaries. Note also that there was some concentration of the δ phase

UNCLASSIFIED
PHOTO 44574

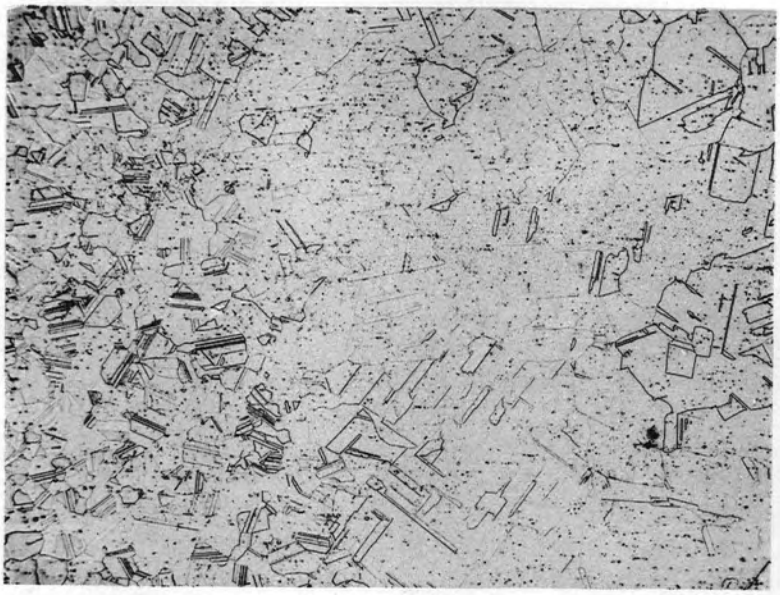

Fig. 28a 50X

Transition in Microstructure Across Heat-Affected Zone

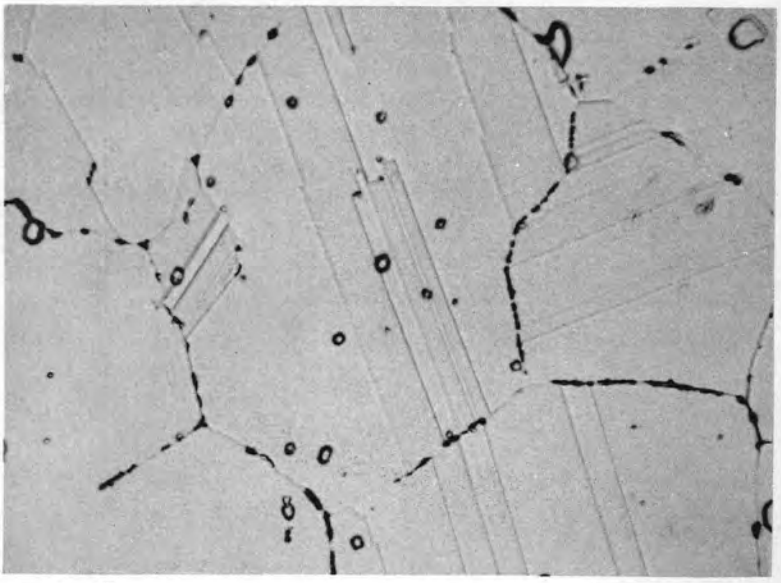

Fig. 28b 1000X

Appearance of Grain Boundaries in Unaffected Base Material

Fig. 28. Microstructure of Hastelloy B Held at 2250°F for 5 Minutes in Argon Atmosphere (Etchant- 1:1:1 HCl, HNO_3, H_2O)

UNCLASSIFIED
PHOTO 44575

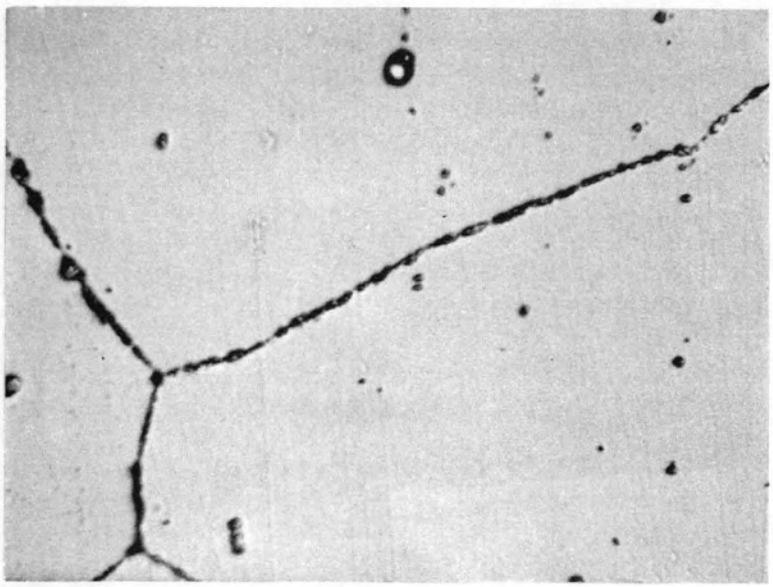

Fig. 28c 1000X

Appearance of Grain Boundaries in Heat-Affected Zone

Fig. 28. Microstructure of Hastelloy B Held at 2250°F for 5 Minutes in Argon Atmosphere (Etchant- 1:1:1 HCl, HNO_3, H_2O)

UNCLASSIFIED
PHOTO 44576

Fig. 29 50X

Microstructure of Hastelloy B Sample Held at 2300°F for 5 Minutes in Argon Atmosphere (Etchant- 1:1:1 HCl, HNO_3, H_2O)

UNCLASSIFIED
PHOTO 44577

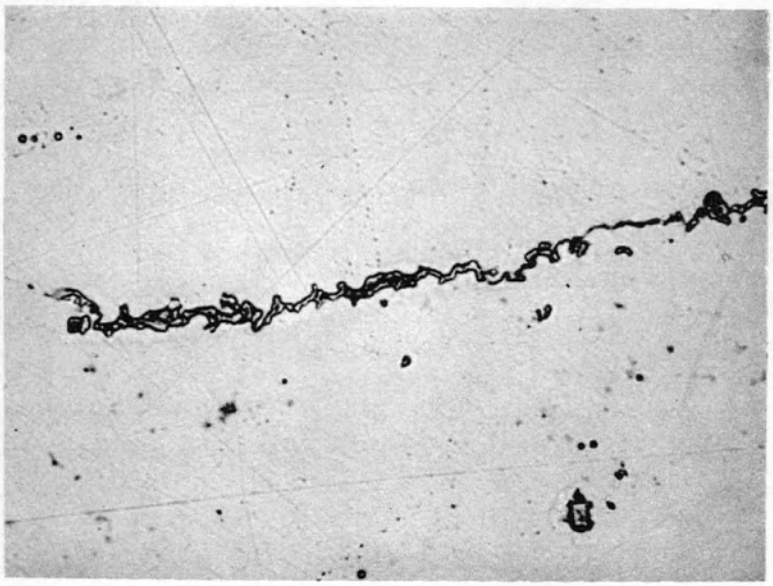

Fig. 30 1000X

Resolvable Grain Boundary Material in Hastelloy B Sample Held at 2350°F for 5 Minutes in Argon Atmosphere
(Etchant- 1:1:1 HCl, HNO_3, H_2O)

UNCLASSIFIED
PHOTO 44578

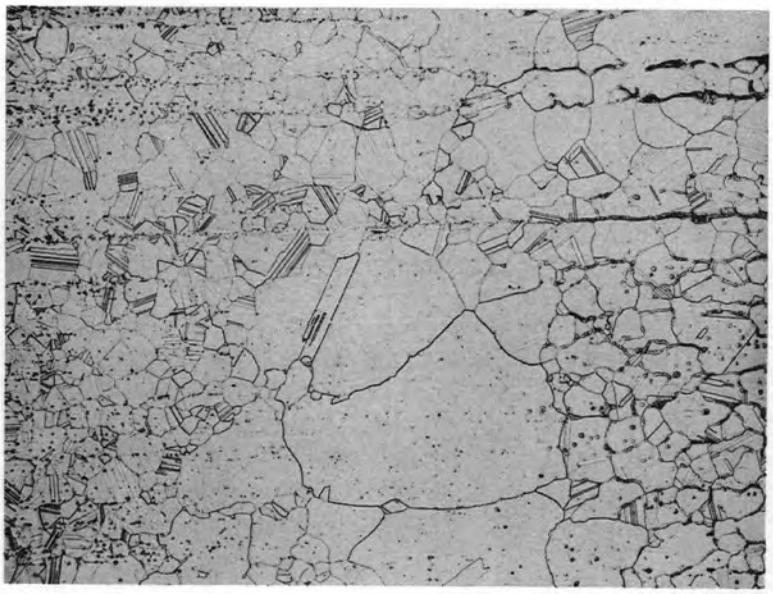

Fig. 31a 50X

Transition in Microstructure Across Heat-Affected Zone

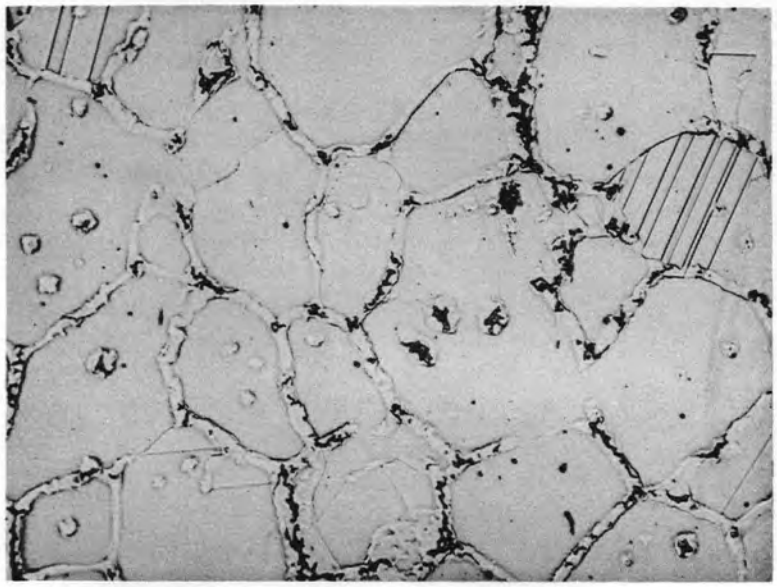

Fig. 31b 250X

Etching Effect Associated with Eutectic

Fig. 31. Microstructure of Hastelloy B Sample Held at 2400°F for 2 Minutes in Argon Atmosphere
(Etchant- 1:1:1 HCl, HNO_3, H_2O)

UNCLASSIFIED
PHOTO 44579

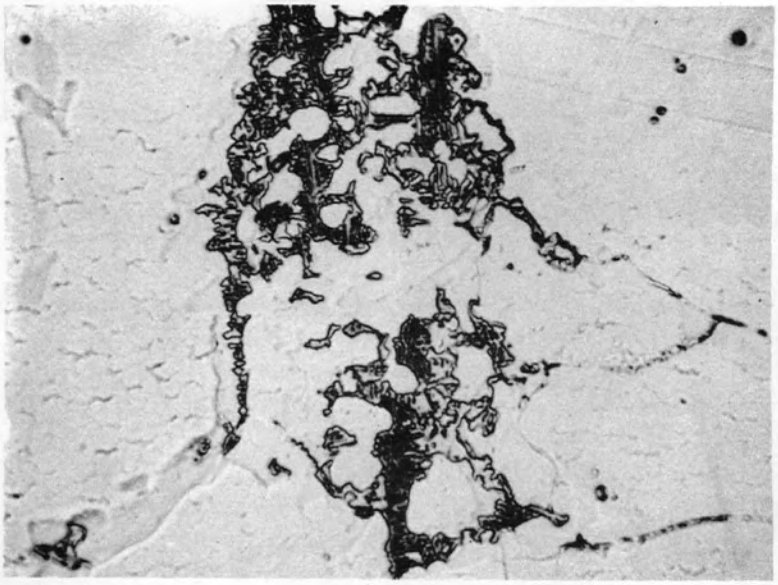

Fig. 31c 1000X

Appearance of Eutectic at High Magnification

Fig. 31. Microstructure of Hastelloy B Sample Held at 2400°F for 2 Minutes in Argon Atmosphere
(Etchant- 1:1:1 HCl, HNO_3, H_2O)

in the base material into heavy stringers. These stringers extend across the grain-coarsened zone and are associated with heavy formations of the eutectic. In these regions, as in the center of the heat-affected zone, grain-coarsening has been retarded.

A differential etching effect associated with the eutectic, both in the grain boundaries and within the grains is shown in Figure 31b.

The appearance of the eutectic at 1000X is shown in Figure 31c. It is quite obviously the same constituent as that produced in samples subjected to a normal 2400°F cycle.

PART VII

DISCUSSION

Since reference will be made to the nickel-molybdenum equilibrium diagram of Figure 1 during this discussion, it would be wise to mention a few points concerning this diagram which are significant with respect to this investigation.

1. The δ phase is an intermetallic compound containing about 62% Mo and having the formula NiMo. It forms by a peritectic reaction at 2500°F.
2. The eutectic, a mixture of α and δ, occurs at a molybdenum content of 46.5%. The eutectic temperature is 2410°F.
3. At the eutectic temperature, the nickel-rich solid solution, α, contains 37% Mo.

If the effect of minor elements in commercial Hastelloy B were assumed negligible, the alloy could be considered as a 60% Ni, 30% Mo composition. According to the phase diagram, Hastelloy B would then be a single phase alloy in the temperature range of 1600°F to 2400°F. Since the peritectoid reactions at low temperatures are sluggish, this single phase structure would probably be retained at room temperature. In actuality, commercial Hastelloy B is a two-phase structure, the matrix being α solid solution containing a secondary phase. It was first thought that the secondary phase was the compound identified by Rosenbaum[11] and the Mond Nickel Company[13] as M_6C. This thought was quickly rejected, since the carbon content of this heat of Hastelloy B was only 0.02%, and the quantity of secondary phase completely excessive for such a carbon content. A more logical assumption was that the secondary phase was the intermetallic compound δ, as it was considered to be by Monkman et al.[10] It is obvious, therefore, that while the Ni-Mo phase diagram may be used as a guide, the presence of approximately 5% Fe and 5% of other alloying elements has the effect of shifting phase boundaries and probably transformation temperatures. Keeping the preceding in mind, it is possible to follow the microstructural changes and their effect on the properties of the alloy.

From Figure 10, the ductility of Hastelloy B samples tested on heating has been unimpaired up to 2250°F. A metallographic study of samples tested at thermal cycles up to 2250°F has shown no change in the as-received structure, correlating with ductility data.

Samples fractured at 2300°F have begun to lose ductility. At this temperature, the presence of grain-boundary films was noted. Further loss in ductility as a result of tests made at 2350°F can be attributed to the increase in the amount of grain-boundary material as a result of increasing the maximum temperature of heat treatment. Should these grain-boundary films be brittle or low melting, they can easily account for the loss in ductility.

The above metallographic features are presented in Figures 22, 23, and 24. The constitution of the grain-boundary films is questionable. However, the prolonged heat treatment at 2350°F given the sample of Figure 30 has produced a grain-boundary film resolvable at 1000X. Judging from the irregular interface characterized by many small cusps, the film was molten at this temperature.

The 2400°F thermal cycle has resulted in a total loss in ductility. An examination of the microstructures resulting from this treatment reveals the reason. The fringes of the heat-affected area where the peak temperature was somewhat less than 2400°F are the transition zones shown in Figure 25a. These zones contain a material having the appearance of coarse "Chinese script". Near the fracture surface, in the area which was actually at 2400°F, there is a much finer distribution of this script material. Actually, both structures are the same constituent except for slight variations in composition. The constituent is a recognized eutectic structure common to some cast aluminum alloys. Ellinger[8] reports such a structure in a 60 Ni, 40 Mo alloy.

What has occurred is a diffusion of Ni from the α phase to the δ phase and a diffusion of Mo in the opposite direction, lowering the melting point of the δ phase (see Figure 1). The effect of the slight thermal gradient across the heat-affected zone on the rate of diffusion and the thermal gradient itself have resulted in only a partial liquefaction of the δ phase in the transition zone and complete liquefaction in the area at

2400°F. On cooling, the δ phase forms from the molybdenum-rich liquid areas, accompanied by simulataneous rejection of nickel. The remaining liquid, enriched with nickel, solidifies as α phase around the δ particles in a eutectic distribution. Over the central region of the heat-affected zone, as a result of the faster cooling rate, the eutectic distribution is a very fine "Chinese script". At the extremes of the heat-affected zone, slower cooling rates prevailed and the eutectic distribution is much coarser.

Since a sample held at 2350°F for 5 min contained a small amount of eutectic, it appears that the minimum temperature of its formation may be deduced to be 2350°F. The presence of this eutectic is responsible for the initial loss in ductility of Hastelloy B. As samples containing this constituent have poor ductility at temperatures 2200°F and above, the eutectic is apparently weaker than the higher melting matrix in this temperature range. Additionally, since the only losses in tensile strength, as compared with results for samples tested on heating, occur in material which contains this eutectic, a Hastelloy B microstructure of eutectic and α is weaker than one of α and δ.

There is some loss in ductility for samples subjected to a 2350°F thermal cycle. The only source of this deterioration in ductility is the grain-boundary films which are extensive as a result of such a heat treatment. These films are apparently brittle or molten at temperatures of 2350°F and higher. At lower temperatures, the strength of these films is such as to cause negligible change in properties. They have no more deleterious effect on tensile strength than the presence of the eutectic.

In all tests, the result of strain measurements indicates that this property of the material is insensitive as a measure of the deterioration of Hastelloy B. Tensile strength results give some indication, but are not as good a criterion as ductility measurements.

While specimens subjected to normal weld thermal cycles exhibit little grain coarsening, the samples held for two to five minutes at elevated temperatures all have been severely grain coarsened. In the temperature range of 2250 to 2350°F (Figures 28, 29, and 30), the entire heat-affected

zone of these samples has undergone germination. In connection with this, there has been some solutioning of δ phase at 2350°F. At 2400°F (Figure 31), a band of extremely coarse grains has formed on either side of the eutectic zone. In this region, the δ phase has gone into solution. In the eutectic zone at the center of the heat-affected zone, very little grain growth has taken place. The formation of liquid eutectic at the grain boundaries has apparently prevented the grains from growing.

The differential etching effect shown in Figure 31b is associated in all cases with the formation of eutectic. It is possible that this effect marks the limits of the liquefied material, and, as solidification occurred with the formation of molybdenum-rich eutectic, the remaining liquid became nickel-rich and was rejected as a band of α surrounding the eutectic. Because of compositional difference from the unmelted matrix, there could result a difference in the attack of etchant used.

PART VIII

CONCLUSIONS

With respect to this investigation, the following may be concluded:

1. A versatile apparatus has been constructed which is presently being used to investigate the properties and microstructures of weld heat-affected zones. With modifications, the equipment can be used to heat, treat, and also test various types of specimens (sheet stock, impact specimens, cylindrical specimens) at a wide range of strain rates and in various atmospheres. The equipment is especially well suited for short-time stress-rupture tests at elevated temperatures.
2. The ductility of Hastelloy B tested on heating increases slightly with testing temperatures up to 2250°F. This is in agreement with studies which show that no microstructural changes have taken place up to 2200°F.
3. The ductility of Hastelloy B tested on heating is impaired by a temperature of 2350°F. This deterioration in ductility is attributed to the presence of grain-boundary films.
4. Hastelloy B tested at 2400°F on heating is completely brittle. Microstructural changes which have resulted in the formation of a eutectic are responsible.
5. Comparison of microstructures of samples held at elevated temperatures for 2 to 5 min with samples subjected to normal weld thermal cycles show that the eutectic forms slowly at 2350°F and rapidly at 2400°F.
6. As indicated by reduction-in-area results for Hastelloy B tested on cooling from 2400°F, the presence of the eutectic severely impairs ductility properties above 2000°F. It must therefore be weak in comparison to the matrix at temperatures above 2000°F.

7. Tensile test results indicate that a microstructure of α and eutectic is weaker than the normal structure of α and δ. The presence of grain-boundary films does not have an injurious effect on tensile strength at any testing temperature.
8. Strain measurements are inadequate as an indication of impairment of the material.
9. From experience gained in similar investigations on other materials, the spreads in experimental data for most testing temperatures were judged excessive for a wrought material. It is suggested that a statistical sample of tensile tests on the as-received material might indicate variable properties. If such is the case, the reason should be sought. One possibility suggested by the sponsor is the susceptibility of the alloy to chemical segregation.

LITERATURE CITED

1. Nippes, E. F. and Savage, W. F., "Development of Specimen Simulating Weld Heat-Affected Zones," The Welding Journal, Vol. 28, p 534-s (1949).

2. Hess, W. F., Merrill, L. L., Nippes, E. F., and Bunk, A. P., "The Measurement of Cooling Rates Associated with Arc Welding and Their Application to the Selection of Optimum Welding Conditions," The Welding Journal, Vol. 22, p 377-s (1943).

3. Hess, W. F., Nippes, E. F., Merrill, L. L., and Bunk, A. P., "Determination of Cooling Rates of Butt and Fillet Welds as a Result of Arc Welding with Various Types of Electrode on Plain Carbon Steel," The Welding Journal, Vol. 23, p 376-s (1944).

4. Rosenthal, Daniel, "A Mathematical Theory of Heat Distribution During Welding and Cutting," The Welding Journal, Vol. 20, p 200-s (1941).

5. Nippes, E. F. and Savage, W. F., "Tests of Specimens Simulating Weld Heat-Affected Zones," The Welding Journal, Vol. 28, p 599-s (1949).

6. Nippes, E. F., Wawrousek, H., and Fleischmann, W. L., "Some Properties of the Heat-Affected Zone in Arc Welded Type 347 Stainless Steel," The Welding Journal, 34, No. 4, 169-s (1955).

7. Nippes, E. F, Savage, W. F., Mason, H. F., Bastian, B. J., and Curran, R. M., "An Investigation of the Hot Ductility of High-Temperature Alloys," The Welding Journal, 34, No. 4, 183-s (1955).

8. Ellinger, F. H., "The Nickel-Molybdenum System," Trans. Am. Soc. Metals, Vol. 30, p 607 (1942).

9. Parke, R. M., "The Molybdenum-Nickel Phase Diagram," Metals Handbook, 1948 Edition, p 1230.

10. Monkman, Jr., F. C., Grant, N. J., and Floe, C. F., Final Report on Development and Testing of Nickel-Molybdenum Alloys, ORNL 1990.

11. Rosenbaum, B. M., "An X-Ray Diffraction Investigation of the Microconstituents in 20 High-Temperature Alloys," Conference on High-Temperature Materials, NACA, p 10 (1947).

12. Badger, Jr., F. S., and Sweeny, Jr., W. O., "Metallurgy of High-Temperature Alloys Used on Current Gas Turbine Designs," Symposium on Materials for Gas Turbines, ASTM, p 99 (1946).

13. Nickel-Molybdenum Alloys, Mond Research Summary, Third Quarter (1955).

14. Savage, W. F., Some Observations on the Hot Ductility of Austenitic Stainless Steels, Doctoral Thesis, p 30 (June 1955).

ORNL-2582
Metallurgy and Ceramics
TID-4500 (13th ed., Rev.)
February 15, 1958

INTERNAL DISTRIBUTION

1. C. E. Center
2. Biology Library
3. Health Physics Library
4. Metallurgy Library
5-6. Central Research Library
7. Reactor Experimental Engineering Library
8-27. Laboratory Records Department
28. Laboratory Records, ORNL R.C.
29. A. M. Weinberg
30. L. B. Emlet (K-25)
31. J. P. Murray (Y-12)
32. J. A. Swartout
33. E. H. Taylor
34. E. D. Shipley
35. M. L. Nelson
36. W. H. Jordan
37. C. P. Keim
38. R. S. Livingston
39. R. R. Dickison
40. S. C. Lind
41. F. L. Culler
42. A. H. Snell
43. A. Hollaender
44. M. T. Kelley
45. K. Z. Morgan
46. J. A. Lane
47. A. S. Householder
48. C. S. Harrill
49. C. E. Winters
50. D. S. Billington
51. H. E. Seagren
52. D. Phillips
53. A. J. Miller
54. R. A. Charpie
55. C. F. Leitten
56. E. G. Bohlmann
57. C. O. Smith
58. M. J. Skinner
59. J. H. Frye, Jr.
60. W. W. Parkinson
61. W. D. Manly
62. J. E. Cunningham
63. G. M. Adamson, Jr.
64. J. W. Allen
65. R. J. Beaver
66. E. S. Bomar, Jr.
67. R. E. Clausing
68. J. H. Coobs
69. J. H. DeVan
70. L. M. Doney
71. D. A. Douglas, Jr.
72. E. A. Franco-Ferreira
73. R. J. Gray
74. J. P. Hammond
75. R. L. Heestand
76. T. Hikido
77-111. M. R. Hill
112. E. E. Hoffman
113. H. Inouye
114. L. K. Jetter
115. C. J. McHargue
116-120. P. Patriarca
121. M. L. Pickelsimer
122. T. K. Roche
123. L. D. Schaffer
124. G. P. Smith, Jr.
125. A. Taboada
126. W. C. Thurber
127. R. C. Waugh
128. H. L. Yakel, Jr.
129. J. H. Koenig (consultant)
130. H. Leidheiser, Jr. (consultant)
131. C. S. Smith (consultant)
132. H. A. Wilhelm (consultant)
133. ORNL - Y-12 Technical Library, Document Reference Section

EXTERNAL DISTRIBUTION

134. Division of Research and Development, AEC, ORO
135-144. Rensselaer Polytechnic Institute, Troy, N.Y.
145-634. Given distribution as shown in TID-4500 (13th ed., Rev.) under Metallurgy and Ceramics category